Journal of Materials Science & Technology

γ" variant-sensitive deformation behaviour of Inconel 718 superalloy

--Manuscript Draft--

Manuscript Number:	J-MST-D-22-00454R1
Full Title:	γ" variant-sensitive deformation behaviour of Inconel 718 superalloy
Short Title:	γ" variant-sensitive deformation behaviour of Inconel 718 superalloy
Article Type:	Research Article
Keywords:	Ni-base superalloys Precipitation strengthening Neutron diffraction Lattice strains Plastic deformation
Corresponding Author:	Hongbiao Dong, PhD University of Leicester UNITED KINGDOM
Corresponding Author Secondary Information:	
Corresponding Author's Institution:	University of Leicester
Corresponding Author's Secondary Institution:	
First Author:	Ruiyao Zhang, Ph.D.
First Author Secondary Information:	
Order of Authors:	Ruiyao Zhang, Ph.D.
	Hailong Qin
	Zhongnan Bi
	Yuanbo Tang
	Jeferson Araujo de Oliveira
	Tung Lik Lee
	Chinnapat Panwisawas
	Shuyan Zhang
	Ji Zhang
	Jun Li
	Hongbiao Dong
Order of Authors Secondary Information:	
Abstract:	Strengthening in Inconel 718 superalloy is derived from dislocation interaction with γ" precipitates, which exist in disk-shape of three possible orientation variants with their {100} habit plane normal to each other. The interactions between dislocations and γ" precipitates vary according to the γ" orientation variants, which makes the deformation behaviour complicated and difficult to reveal experimentally. In this work, γ" variant distributions of Inconel 718 samples were tailored by ageing heat treatment under either a tensile or compressive stress. The γ" variant-sensitive deformation behaviours were then studied by in-situ tensile test via neutron diffraction at room temperature. It is demonstrated that yielding first takes place in grains oriented with <110> parallel to the loading direction. An identical lattice strain response to applied stress of both the γ matrix and the γ" precipitates was observed during yielding, suggesting dislocations shearing through the g^2 precipitates is predominant at this stage. Variations in yield strength for samples with different γ" variant distributions

	were observed, which can be attributed to different strengthening that arises from interactions between dislocation and different γ" variants.
Suggested Reviewers:	Yandong Wang University of Science and Technology Beijing ydwang@ustb.edu.cn He is an expert in neutron diffraction field with experience working in neutron diffraction facility and research on relevant topics.
	Jonathan Cormier ISAE-ENSMA jonathan.cormier@ensma.fr He is an expert in the field of Ni-base superalloys.
	Timothy Smith National Aeronautics and Space Administration: NASA timothy.m.smith@nasa.gov Dr smith has rich experience in research on Ni-base superalloys.
Opposed Reviewers:	
Response to Reviewers:	
Additional Information:	
Question	**Response**

γ″ variant-sensitive deformation behaviour of Inconel 718 superalloy

R.Y. Zhang [a, b, 1, *], H.L. Qin [c, 1], Z.N. Bi [c], Y.T. Tang [d], J. Araújo de Oliveira [e], T.L. Lee [f], C. Panwisawas [b], S.Y. Zhang [a], J. Zhang [c], J. Li [g], H.B. Dong [b, *]

[a] *Centre of Excellence for Advanced Materials, Dongguan, 523808, China*

[b] *School of Engineering, University of Leicester, University Road, Leicester LE1 7RH, UK*

[c] *Beijing Key Laboratory of Advanced High Temperature Materials, Central Iron and Steel Research Institute, No. 76 Xueyuannanlu, Haidian, Beijing, 100081, China*

[d] *Department of Materials, University of Oxford, Parks Road, Oxford OX1 3PH, United Kingdom*

[e] *StressMap, Engineering and Innovation Department, The Open University, Walton Hall, Milton Keynes MK7 6AA, UK*

[f] *ISIS Neutron Source, Rutherford Appleton Laboratory, Harwell Science and Innovation Campus, Chilton, Oxfordshire, OX11 0QX, UK*

[g] *School of Material Science and Engineering, Shanghai Jiao Tong University, Shanghai, 200240, China*

[1] These authors contributed equally to this work and should be considered co-first authors: R.Y. Zhang, H.L. Qin

* Corresponding authors: (R.Y. Zhang) Email address: ruiyao.zhang@ceamat.com, (H.B. Dong) Tel: +44 116 2522528, Email address: hd38@le.ac.uk

Abstract

Strengthening in Inconel 718 superalloy is derived from dislocation interaction with γ″ precipitates, which exist in disk-shape of three possible orientation variants with their {100} habit plane normal to each other. The interactions between dislocations and γ″ precipitates vary according to the γ″ orientation variants, which makes the deformation behaviour complicated and difficult to reveal experimentally. In this work, γ″ variant distributions of Inconel 718 samples were tailored by ageing heat treatment under either a tensile or compressive stress. The γ″ variant-sensitive deformation behaviours were then studied by *in-situ* tensile test via neutron diffraction at room temperature. It is demonstrated that yielding first takes place in grains oriented with <110> parallel to the loading direction. An identical lattice strain response to applied stress of both the γ matrix and the γ″ precipitates was observed during yielding, suggesting dislocations shearing through the γ″ precipitates is predominant at this stage. Variations in yield strength for

samples with different γ″ variant distributions were observed, which can be attributed to different strengthening that arise from interactions between dislocation and different γ″ variants.

Keywords: Ni-base superalloys, Precipitation strengthening, Neutron diffraction, Lattice strains, Plastic deformation

1. Introduction

Inconel 718 (IN718) has been one of the most widely used Ni-base superalloys in aeroengines, nuclear and oil & gas industries for decades [1,2], and has become a popular candidate for applications in additive manufacturing nowadays [3–6]. Its popularity is attributed to the excellent mechanical properties at elevated temperatures up to 650 °C, remarkable good weldability and machinability plus relatively low cost. IN718 derives strengthening from the presence of γ′ and γ″ precipitates that are embedded in the γ matrix [7]. The γ matrix phase displays a disordered face-centred cubic (FCC) structure, the γ′ phase possesses a $L1_2$ ordered structure and the γ″ phase has a $D0_{22}$ body-centred tetragonal (BCT) structure [1]. It has been suggested that the major strengthening phase in IN718 is the γ″ owing to its larger volume fraction compared to the γ′ phase [8–10].

The γ″ phase maintains a cube-cube orientation with the γ matrix, or $\{100\}_{\gamma''}//\{100\}_{\gamma}$ and $[100]_{\gamma''}//<100>_{\gamma}$ [1]. The γ″ has a relatively large lattice misfit of ~3% with the γ along the *c-axis*, while a smaller misfit of <1% with the γ along the *a-axis*. The different lattice misfits consequently result in the occurrence of disk-shaped γ″ precipitates in three orientations with the disk plane normal to each other [11].

Misfit between the phases not only determines the morphology of the precipitate but also plays an important role in affecting the coherency strengthening in IN718 [8]. During deformation, the localized stresses in the precipitate-matrix system will interact with dislocation motions and significantly affect the deformation behaviour. Understanding the deformation mechanisms of precipitation strengthening materials is necessary in predicting the mechanical properties and achieving an optimum performance. For precipitation hardening Ni-base superalloys, strengthening is achieved by impeding the motion of dislocations by the coherent precipitates. At room temperature, dislocation shearing or bowing around the coherent precipitates are the dominant strengthening mechanism. For the γ″-Ni-base superalloys, such as IN718, the deformation mechanisms

are complicated due to the tetragonal crystal structures of the γ″. Oblak *et al*. [8] suggested the appearance of quadruplets 1/2<110> dislocations which shear the three γ″ variants and restore the order of the γ″ structure in an underaged IN718 sample. Chaturvedi and Han [10] reported that the dislocations appeared in pairs in underaged IN718 samples. Sundararaman *et al*. [9] proposed a transition of deformation mechanism from shearing by dislocations movements to shearing by the passage of true crystallographic deformation twins when the γ″ precipitates exceed a critical size (~10 nm). Recent studies using phase field simulation technique uncovered a variety of sophisticated deformation mechanisms that involve unique interactions between dislocations and an individual γ″ variant [12–14]. Although these investigations show inconsistency on the observed deformation mechanisms, clearly, they all suggest the deformation mechanism is variant dependent. Indeed, recent studies have shown the mechanical property of IN718 can be enhanced by tailoring the γ″ variant distribution [15–18].

Thanks to the developments of neutron sources and strain-scanning beamlines, *in situ* neutron diffraction has become a powerful complementary method to microstructure observations in studying the elastic properties and deformation mechanisms of crystalline materials [19,20,29,21–28]. In contrast to a TEM observation, which only provides post-mortem microstructures on very small material volumes, neutron diffraction reveals the evolution of *hkl* plane-specific lattice strains sampled from a relatively large gauge volume (~ tens of mm^3) during testing. For multi-phase materials, the phase-specific lattice strains can be obtained, provided that the diffraction patterns from the constituent phases are distinguishable.

However, challenges remain in studying γ″ when using neutron diffraction due to its low volume fraction, three variants distribution, and diffraction peaks overlapping. In order to tackle the difficulties, the stress-induced variant selection (SIVS) method was applied in this study. The γ″ precipitates experience SIVS when either a tensile or compressive stress is applied to IN718 during the ageing heat treatment stage. During ageing, the applied stress interacts with the misfit strain of the γ″ particles and leads to a change in strain energy, which can be simplified as [30]:

$$\Delta E = -\sigma \times \varepsilon_c \times cos^2\theta \times V \quad (1)$$

, where σ is the applied stress, ε_c is the transformation strain along *c-axis*, θ is the angle between the *c-axis* and the stress axis, and V the volume of the γ″ variant, as illustrated in Figure 1. In an individual grain, if a variant's θ is smaller compared to that of other

variants, this variant will be promoted in the case of a tensile stress applied, or suppressed when a compressive is applied. In terms of the extent of variant selection, it is a function of grain orientation, sign and magnitude of applied stress, ageing temperature and duration of ageing. For an example, a grain with its [111] parallel to the stress axis will experience no variant selection, as the θ is identical for all three variants. While an [100] oriented grain is the most vulnerable to variant selection, as θ is 0° for one variant and 90° for the remaining two. The detail study of variant selection related to temperature, stress and grain orientation can be found in ref. [16]. Following the SIVS ageing heat treatment, the samples with selected variant distributions were taken to ENGIN-X Time-of-Flight neutron diffractometer for in-situ tensile experiment. The benefits of selected γ″ variant distributions in the current study is twofold: first, it makes the γ″ diffraction peak discernible from neutron diffraction. For a sample without variant selection, two diffraction peaks of gamma double prime exist due to the different lattice parameters along a- and c-axes. In contrast, for a variant selected sample, the gamma double prime diffraction peak includes all the intensity arises from the precipitates' volume in these grains and have higher intensity [30–32]. And second, it makes the contributions of different γ″ variants in strengthening distinguishable and thus their respective effect are studied.

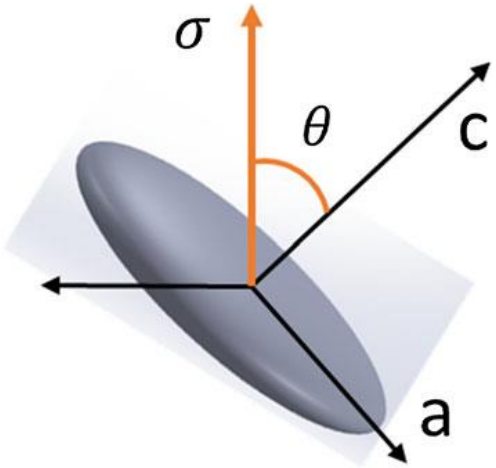

Figure 1. An illustration of the angle θ between stress axis and *c-axis* of a γ″ precipitate [30].

2. Methodology

2.1. Sample preparation

In the current study, polycrystalline IN718 alloy with a nominal chemical composition listed in Table 1 was used. The alloy was manufactured via vacuum induction melting, electro-slag re-melting and vacuum arc re-melting processes. The ingot underwent high temperature homogenization with 1160 °C / 24 h + 1190 °C / 72 h + air cooling, before radially forging into a bar in 220 mm diameter. Rod specimens were extracted from the forged IN718 bar and then solution heat treated at 980 °C for 1 hour followed by forced-air cooling to RT. Rod specimens were machined to test bars with M12 thread heads, 42 mm gauge length and 8 mm gauge diameter. Finally, test bars were subjected to ageing heat treatment at 790 °C for 5 hours either with a 300 MPa tensile or compressive stress applied, which resulted in γ″ variants selected.

Substantial research has shown during ageing heat treatment when the platelet precipitation happens, an applied stress will have an impact on the selection of the orientation variant of the precipitates. These studies have proposed that the variant selection is resulted from the different interaction energies between an applied stress and transformation strains of different variants [8,33–36]. The favoured growth and coarsening happens to the variant that has the most reduction in strain energy. The volume fraction of the selected variant is increased at the expense of the other variants. The benefits of selected γ″ variant distribution in the current study is twofold: first it makes the γ″ diffraction peak become discernible from neutron diffraction [30–32], and second it makes the contributions of different γ″ variants in strengthening distinguishable and thus their respective deformation behaviour during tensile loading can be studied.

Table 1. Chemical composition of IN718 alloy (in w.t.%)

C	Cr	Nb	Ti	Al	Mo	Fe	Ni
0.023	18.05	5.42	0.91	0.48	2.90	18.00	Balanced

2.2. Microstructure characterization

Microstructure characterization focusing on the γ″ variant distribution after ageing heat treatment was performed on the cross-section of the test bars. The characterization was carried out using a JSM-7800F (JEOL, Japan) scanning electron microscope (SEM) equipped with electron backscatter diffraction (EBSD). The FE-SEM samples were electro-polished at 20 V in an electrolyte solution of 20 %H_2SO_4+80 % CH_3OH, followed

by etching in a solution of 150 ml H_3PO_4+10 ml H_2SO_4＋15 g CrO_3. Crystal orientation mappings were first performed, then secondary electron imaging mode was used to characterize the γ″ variant distribution in the grains oriented with <110>, <100> and <111> closely parallel to the loading direction.

2.3. *In situ* neutron diffraction experiment

The *in situ* neutron diffraction tensile deformation experiment was performed using the ENGIN-X time-of-flight neutron diffractometer at ISIS neutron pulse source, UK [37]. The bar sample was horizontally mounted on a stress-rig (INSTRON, 100 kN) with its longitudinal direction at 45° relative to the incident neutron beam. Two banks of detectors were located at 2θ = ±90°, allowing *d*-spacing along the longitudinal and transverse directions to be measured simultaneously. In order to maximise diffracted signal, a large nominal gauge volume (NGV), defined by the incident beam slit (10 mm in height and 4 mm in width) and the radial collimator (4 mm), was used. Since the NGV was not fully immersed in the sample, the sample was carefully positioned to ensure the centroid of the NGV lied on the axial line of the sample to minimize pseudo-strain effects. Tensile loading was applied under stress control mode with a stress rate of 10 MPa/s and held at each measurement point. Diffraction measurement was performed at every 200 MPa with an acquisition time of 20 minutes during the elastic regime. Measurement points were increased by reducing the load steps to every 50 MPa when the applied load reached 800 MPa, which is around the yield point. The experimental setup is illustrated in Figure 2.

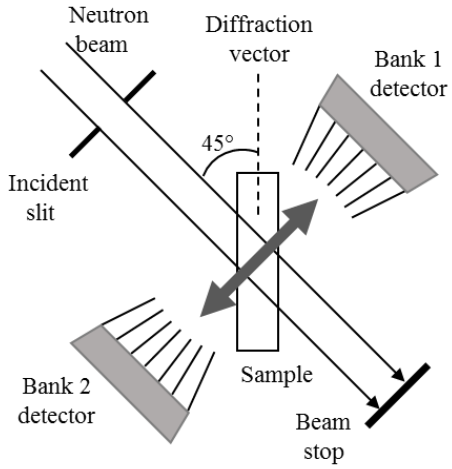

Figure 2. Schematic illustration of in situ neutron diffraction tensile deformation experiment in ENGIN-X, ISIS neutron source, UK.

3. Results

3.1. Selected variant distribution

Inverse pole figures (IPF) viewed along *Z*-axis, which is consistent with the loading direction, are shown in Figure 3a & e for the tensile-aged (hereinafter TA sample) and compressive-aged (CA sample) samples, respectively. Figure 3b-d show the γ″ variant distribution in grains labelled with 'b', 'c' and 'd' in Figure 3a, which are oriented closely to <111>, <100> and <110> directions, respectively. Similarly, Figure 3f-h show the variant distribution in the CA sample. The γ″ variants are represented with different colour shown in the insets with their orientation relationship with the matrix. For the <111> oriented grain shown in Figure 3b, the three variants present in approximately equal quantities. For the <100> oriented grain in Figure 3c, only the variant with the disk-plane perpendicular to the observation direction presents. For the <110> oriented grain in Figure 3d, two orientationally equivalent variants present. For the <111> oriented grain shown in Figure 3f, the three variants present in approximately equal quantities as in Figure 3b. For the <100> oriented grain in Figure 3g, two variants whose disk-plane normal to each other and parallel to the observation direction present. For the <110> oriented grain Figure 3h, only the variant whose disk-plane parallel to the observation direction presents. From all six micrographs, the averaged long axis of the γ″ precipitate is measured to be 56 ± 5 nm, with no significant difference between grains or the two samples. Beside the γ″ precipitates, smaller spherical particles in diameters less than 30 nm are observed, which are believed to be the γ′ precipitates. Literature [38,39] report the volume fraction of γ″ phase is generally not greater than 15%, while the micrographs show a large density of γ″ precipitates with its volume fraction looks very high. This is because the micrographs were taken after electropolishing that have eliminated gamma matrix and may have exposed multi-layers of precipitates.

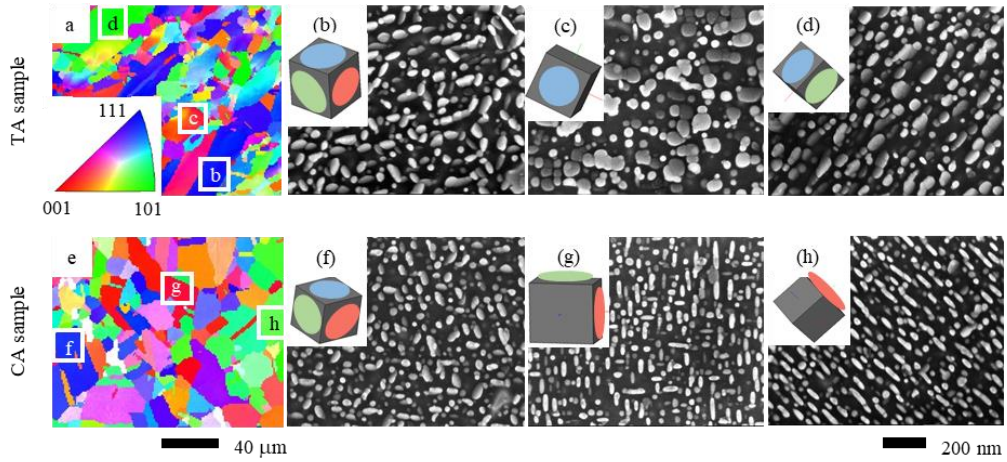

Figure 3. (a) IPF along Z-axis on the cross-section of the TA sample, (b)-(d) γ″ variant distribution in grains selected from locations indicated in (a), (e) IPF on the cross-section of the CA sample, (f)-(h) γ″ variant distribution in grains selected from locations indicated in (e). Insets show the orientation of existing γ″ variants (indicated as either coloured ellipse or circle) with habit planes lying on different faces of the grey cube according to the {100}γ″//{100}γ and [100]γ″//<100>γ relationship with the matrix phase.

3.2. Diffraction pattern and fitting

Diffraction patterns obtained by bank 1 detectors at RT before loading for both the TA and CA samples are shown in Figure 4. One can see the four major peaks ({111}, {200}, {220} and {311}) from the γ phase. Two peaks from the δ phase are also noticed in the patterns. Comparing the two patterns, it is noted that peaks from the γ″ phase ({004}, {204} and {116}) are captured in the pattern for the TA sample, but are not apparent in the pattern for the CA sample. {112} γ″ peak presents at the right shoulder of the {111} γ peak in both patterns.

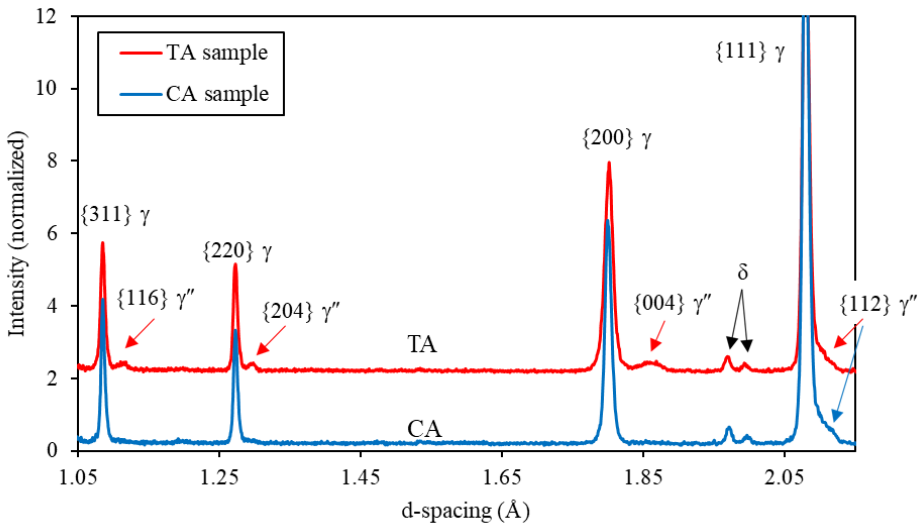

Figure 4. Diffraction patterns obtained along the loading direction at room temperature (RT) before loading of both tensile-aged (TA) and (compressive-aged) CA samples. Small {116}{204}{004} γ" peaks are discerned in TA sample but not in CA sample.

The differences between the two diffraction patterns related to the γ″ phase are attributed to the different γ″ variant distribution in the two samples. For example, Figure 5 illustrates the diffraction on <100> oriented grains in the two samples. In the <100> oriented grains of the TA sample, only the variant with the disk-plane perpendicular to the longitudinal direction presents. Diffraction from this variant contributes to the {004} γ″ peak, which is located at the right of the {200} γ peak due to the larger lattice parameter of the γ″ phase than the γ phase. In contrast, in the <100> oriented grains of the CA sample, only the variants with its disk-plane parallel to the longitudinal direction present. Diffraction from these variants contributes to the {200} γ″ peak. Since the lattice parameter of the γ″ phase is very close to that of the γ phase along its a-axis, the {200} γ″ peak overlaps with the {200} γ peak. Similar diffraction happens to the <110> and <311> oriented grains.

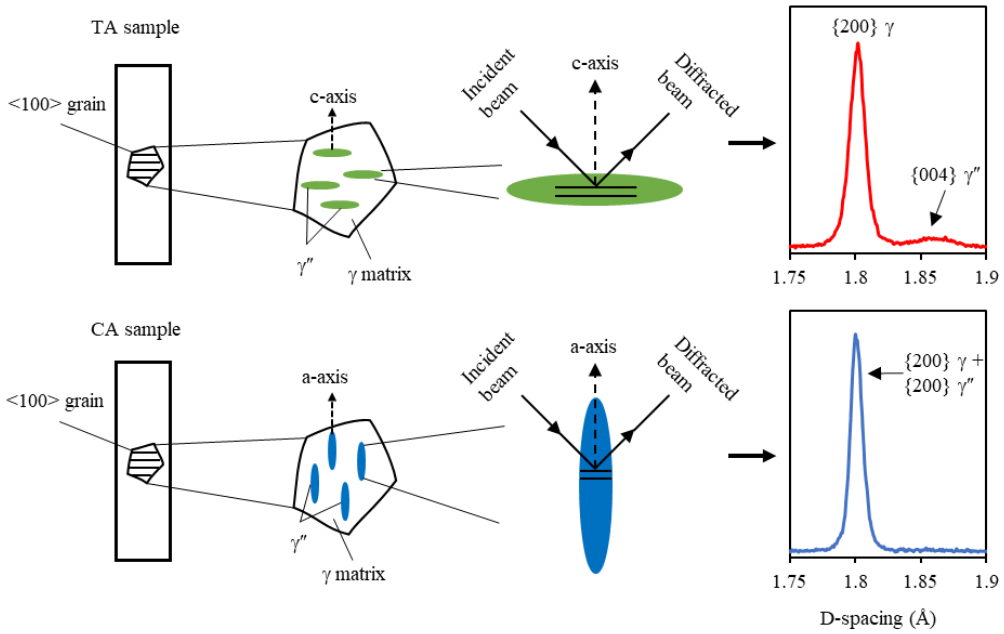

Figure 5. Schematic illustration of diffraction from a <100> oriented grain in (tensile-aged) TA and (compressive-aged) CA samples, respectively, viewing along the transverse direction of the bar sample. Non-overlapping {004} γ" peak are contributed from the variant with c-axis parallel to diffraction vector while the {200} overlapping peak are from the variant with a-axis parallel to the diffraction vector.

Since the γ″ peaks are discernible in the TA diffraction pattern, diffraction peaks of both the γ and γ″ peaks were fitted by using Pseudo-Voigt functions [40–42]. γ′ peaks were not considered to have large influences on the current peak fitting due to its low volume fraction and close lattice parameter to that of the γ phase. The non-overlapping γ and γ″ peaks were fitted as shown in Figure 6a-c, the respective γ-to-γ″ intensity ratio were then obtained. For the CA sample where the γ and γ″ peaks are overlapped, peak deconvolution using two peak functions was performed. The γ-to-γ″ peak intensity ratio was constrained to the value obtained from the non-overlapping peaks from the TA sample, leaving other fitting parameters free to fit. Such an approach worked well for the three peaks shown in Figure 6d-f except for the {111}γ/{112}γ″ partially overlapping peak. Diffraction peaks obtained at each stress increment were fitted using the same procedure. The fitting sensitivity to the constrained intensity ratio was checked by trying various values with +/-10% off. It resulted in a small shift of d-spacing of the γ″ peak, but the small shift was cancelled out when lattice strain evolution was considered. Therefore, the fitting method was considered reliable for the current study.

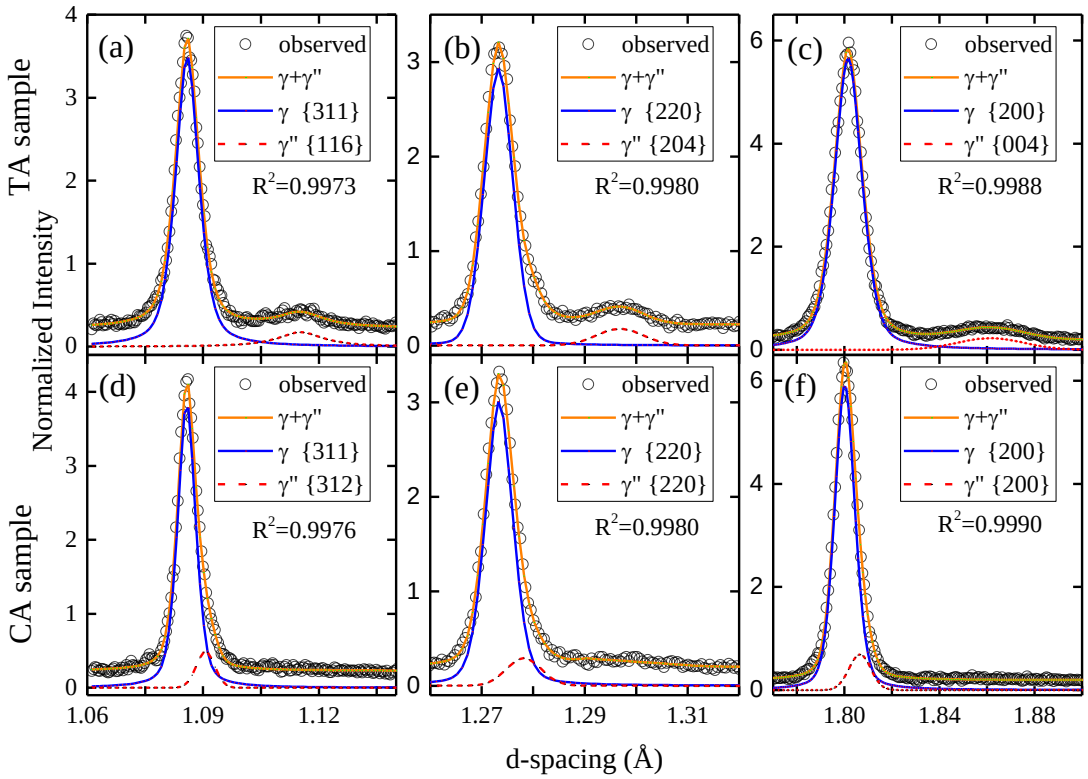

Figure 6. Fitting of diffraction peaks for (a) – (c) non-overlapping peaks for tensile-aged (TA) sample, and deconvolution results for (d) – (f) overlapping peak for compressive-aged (CA) sample, showing the accuracy of the fitting.

3.3. Elasticity of γ″

The *d*-spacing d_{hkl} of each *hkl* reflection for both the γ and γ″ phases were obtained from fitting each *hkl* reflection. The elastic lattice strain was calculated by:

$$\varepsilon_{hkl} = \frac{d_{hkl} - d^0_{hkl}}{d^0_{hkl}} \quad (2)$$

, where d^0_{hkl} is the *d*-spacing for a specific *hkl* reflection measured at the beginning of the test. The lattice strain against applied stress at the elastic regime is obtained and plotted in Figure 7. The DEC of each *hkl* reflection E^{hkl} of both phases was obtained by linearly fitting each of the plot. The results are listed in Table 2 and Table 3.

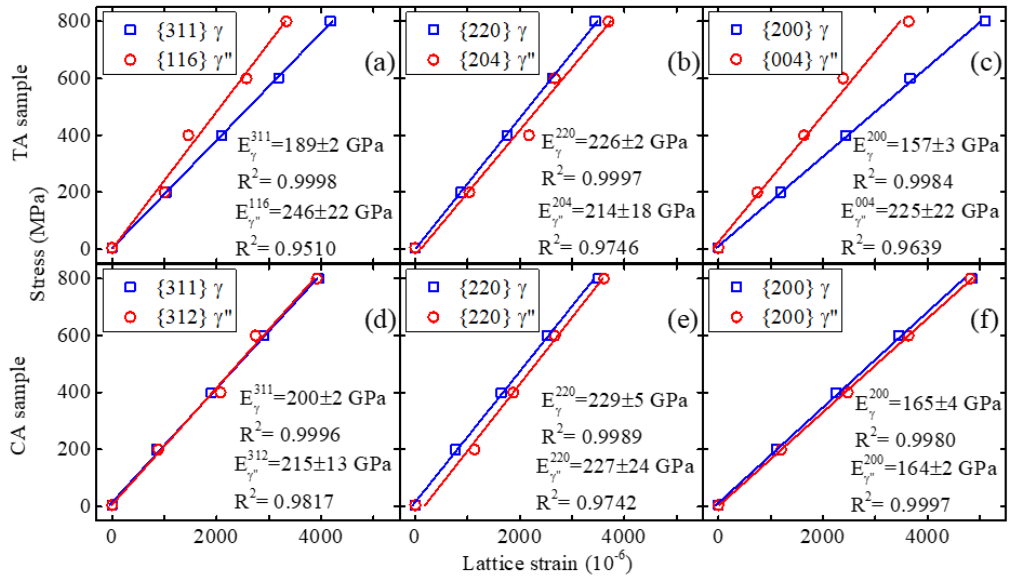

Figure 7. Stress-lattice strain plots for each *hkl* relfection of both the γ and γ″ phases in the elastic regime. (a) – (c) for tensile-aged (TA) sample, (d) – (f) for compressive-aged (CA) sample. Diffraction elastic constants were obtained by linearly fitting to each of the plot. It is shown the γ" is stiffer along its c-axis (<004> direction) than a-axis (<200> direction), as well as stiffer than the matrix phase. Errors bars associated with the fitting uncertainties are about the size of the symbol and not shown for clarity.

Table 2. Diffraction elastic constant for each *hkl* reflection of the γ″ phase, uncertainties associated with the linear fitting are given. *hkl* reflections for the TA sample are indicated as (TA) while for the CA sample are indicated as (CA).

hkl of γ″	312 (CA)	116 (TA)	220 (CA)	204 (TA)	200 (CA)	004 (TA)
E^{hkl} (GPa)	215	246	227	214	164	225
Uncertainty (GPa)	13	22	24	18	2	22

Table 3. Diffraction elastic constant for each *hkl* reflection of the γ phase, uncertainties associated with the linear fitting are given.

hkl of γ	311 (CA)	311 (TA)	220 (CA)	220 (TA)	200 (CA)	200 (TA)
E^{hkl} (GPa)	200	189	229	226	165	157
Uncertainty (GPa)	2	2	5	2	2	3

The γ″ possesses a BCT crystallographic structure, the DECs along the a-axis and c-axis are different as comparing the E^{004} with the E^{200} (225 GPa vs 164 GPa), bearing in mind that {004} plane is normal to the c-axis, while {200} plane is normal to the a-axis. The difference implies that the $D0_{22}$ γ″ is stiffer along its *c-axis* than along the *a-axis*, although the constraints imposed on each grain/phase of a multi-phase polycrystalline material mean that the DECs do not represent the intrinsic elastic properties. In contrast,

292 the E^{204} and E^{220} of the γ″ phase show no significant differences. By comparing the
293 DECs of the γ″ with those of the γ phase (Table 3), it is shown that the γ″ is stiffer than
294 the γ matrix phase ($E_{\gamma''}^{116}$ vs E_{γ}^{311} and $E_{\gamma''}^{004}$ vs E_{γ}^{004}).
295
296 3.4. Macroscopic stress-strain curves
297 The applied stress-strain curves for the two samples recorded during in situ neutron
298 diffraction tensile experiment are displayed in Figure 8. Note that the complete curves are
299 not shown due to the extensometer slipped at large plastic strain, the fracture took place
300 at an applied stress of 1289 MPa and 1342 MPa for the TA and CA samples, respectively.
301 The CA sample exhibits a larger yield strength and tensile strength than the TA sample.
302 The variation in strengthening by different stress-ageing processes are confirmed by
303 tensile experiment performed in accordance with the ISO 6892-1 2011 standard, and also
304 agrees well with those reported by Qin *et al*. [15]. The 0.2% yield strength and tensile
305 strength are listed in Table 4. The 0.2% yield strength of the in-situ neutron diffraction
306 tested samples are higher compared to their counterpart tested in-house, this can be
307 attributed to the step manner loading during the in situ experiment, although the tensile
308 strength are similar. The microstructures of the two samples are similar in terms of grain
309 size, γ″ precipitate volume fraction and size, and presence of the δ, the major difference
310 is the different stress-induced γ″ variant distribution. Therefore, it is reasonable to
311 speculate that the differences in mechanical performance are due to the different γ″ variant
312 distributions, details are to be discussed in Section 4.2.

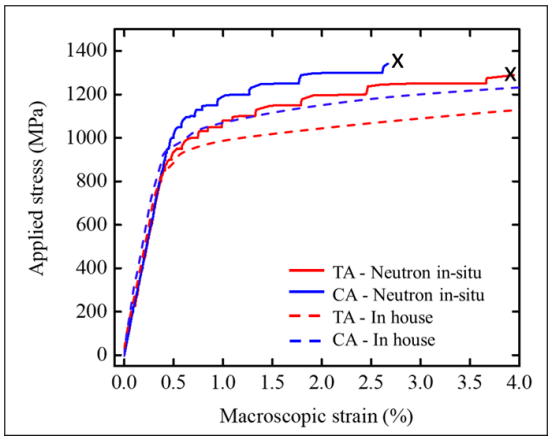

313
314 Figure 8. Applied stress-strain curves for quasi-static in situ neutron tensile deformation
315 and in house laboratory tensile deformation of the two differently aged sample. The ‘x’
316 marker shows the point where the extensometer slipped.
317

Table 4. Summary of 0.2% yield strength and tensile strength of the two differently aged samples tested by in situ neutron diffraction experiment and in house tensile experiment.

	TA - Neutron	CA - Neutron	TA – In house	CA – In house
0.2% yield strength (MPa)	990	1095	910	1000
Tensile strength (MPa)	1289	1342	1245	1322

3.5. Lattice strain evolution

The γ phase *hkl*-specific lattice strain evolutions measured along the longitudinal are shown in Figure *9* a&b. The stress-lattice strain curves give the lattice response to the applied stress during the tensile deformation, which reveal the deformation behaviour at the grain scale. The stress-lattice strain curves for the two samples are similar, showing that the 111 and 311 reflections maintain linearity through the deformation, while 200 and 220 reflections possess nonlinearity at some stage. The nonlinearities are brought about by changes in the intergranular stresses. 220 reflections show reduced strain accumulation, while 200 reflections show increased strain accumulation after the onset of the nonlinearities. The onset of nonlinearity of 220 reflections characterize the onset of crystallographic slip in the <110> oriented grains, and therefore acts as an indicator of the onset of plasticity at the microscale. The onset of nonlinearity of 220 reflection for the TA sample is observed to be at 900 MPa, while for the CA sample, it is 1000 MPa. These onsets of nonlinearity match well with that of the macroscopic stress-strain curves in Figure 8.

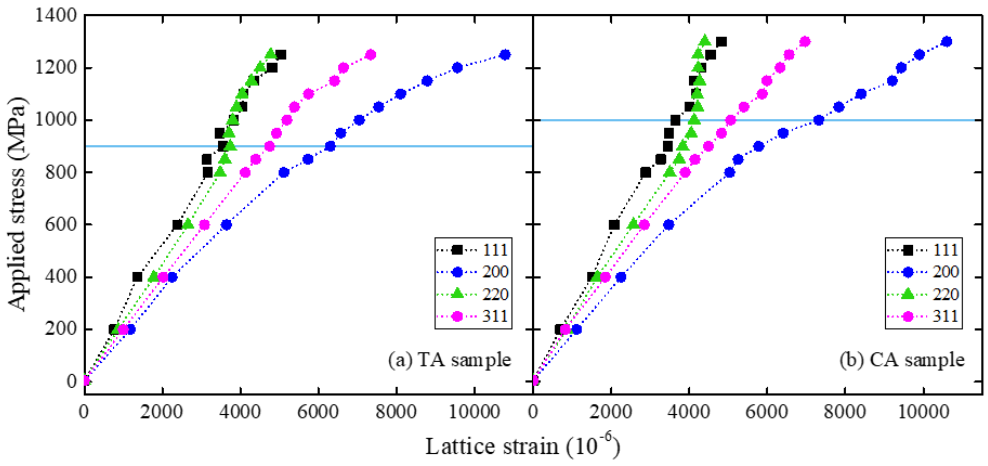

Figure 9. Evolution of *hkl*-specific lattice strain of the γ phase along the longitudinal direction for (a) tensile-aged (TA) and (b) compressive-aged (CA) samples. The horizontal lines indicate the onsets of nonlinearity, which coincide with the 0.2% yield strength obtained from macro stress-strain curves. The error bars associated with uncertainties from peak fitting are about the size of the symbol and not shown here for clarity.

Figure 10 shows the lattice strain evolution of both the γ and γ″ phases in the <100> and <110> oriented grains along the loading direction during deformation.

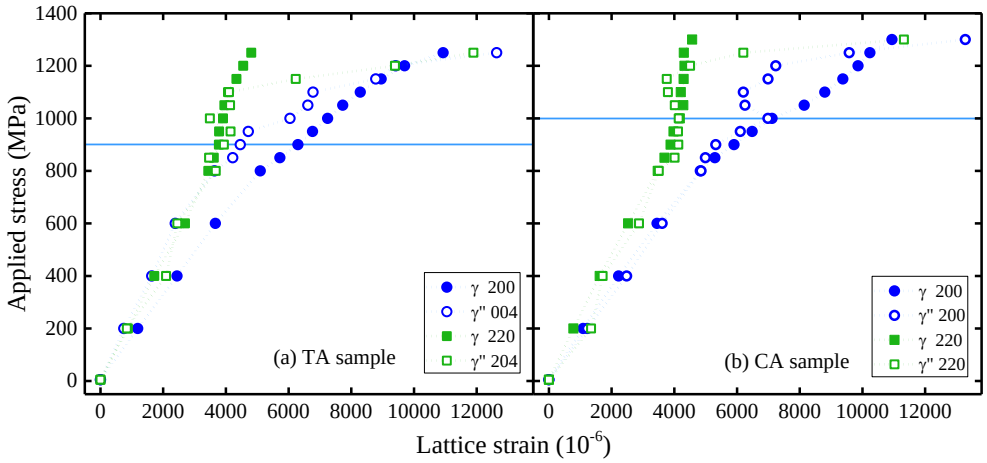

Figure 10. Lattice strain evolution of the γ and γ″ phases for (a) tensile-aged (TA) and (b) compressive-aged (CA) samples during tensile deformation. The horizontal lines indicate the onsets of nonlinearity. Error bars associated with uncertainties of peak fitting are about the size of the symbol in the elastic regime for both phases, and increase from 200 to 1200 microstrains in the plastic regime for the γ″, 100 to 360 microstrains for the γ phase. Error bars are not shown for clarity.

The lattice strain responses can be summarized:

(i) In the <110> oriented grains of the TA sample (green plots in Figure 10a), the γ″ lattice strain increases similarly to that of γ in elastic regime and at early stage of plastic deformation up to 1100 MPa. With further loading, the γ″ phase experienced a larger strain accumulation compared to the γ phase.

(ii) Similarly, in the <110> oriented grains of the CA sample (green plots in Figure 10b), the γ″ lattice strain increases with that of γ in the elastic regime and at the early stage of plastic deformation up to 1200 MPa. With further loading, the γ″ phase experienced a larger strain accumulation compared to the γ phase.

(iii) In contrast, in the <100> oriented grains of the TA sample (blue plots in Figure 10a), the γ″ lattice strain evolution separates from that of the γ phase

in the elastic regime, which is due to the different elasticity as pointed out previously. Both phases experienced increased strain accumulation during plastic deformation.

(iv) In the <100> oriented grains of the CA sample (blue plots in Figure 10b), the γ″ lattice strain increases together with the γ up to 1000 MPa. Then the γ″ phase accumulates little strain increase between 1000 and 1200 MPa, followed by strain accumulation again until fracture. The γ phase keep accumulating elastic strain until fracture.

3.6. Peak width evolution and grain rotation

In addition to the lattice strain evolution, the peak broadening during tensile deformation provides important information to understand the plastic deformation. The evolutions of normalized full width at half maximum intensity (FWHM) of the γ and γ″ reflections from the <100> and <110> oriented grains of the two samples are shown in Figure 11a & b. Peak broadening can have several origins associated with the microstructure of the sample, including nano-sized particle, dislocations, stacking faults, microstrain, and steep macrostrain gradient [40]. Peak broadening during plastic deformation can be attributed to: (i) dislocations and stacking faults break the entity of a crystalline particle, leading to a smaller diffracting size and resulting in particle size broadening, (ii) dislocations and stacking faults generate type-III microstrain fields that give rise to broadening, (iii) grain interaction stresses caused by plastic anisotropy [40]. The dislocations and stacking faults related peak broadening is grain orientation specific since they may preferentially occur in specifically oriented grains during plastic deformation. Whilst, the grain interaction stresses peak broadening is not highly dependent on orientation. Therefore, the peak broadening can act as a qualitative indicator of plastic deformation.

In Figure 11a & b, it is shown that negligible peak broadening occurs in the elastic regime. The onset of noticeable peak broadening closely correlates with the onset of the nonlinearities of lattice strain evolution. The peak broadening of γ reflections are similar to each other, but not as significant as the broadening of γ″ reflections. For the TA sample (Figure 11a), 204 γ″ reflection broadens more significantly than the 004 γ″ reflection. For the CA sample (Figure 11b), both γ″ reflections broaden significantly. The peak

broadening associated with plastic deformation of specific γ″ variants during tensile loading is discussed in section 4.1.

Grain rotation occurred during plastic deformation as a result of slip. The grain rotation can be observed by the evolution intensity of the γ reflections, as shown in Figure 11c & d. The intensity of each peak remained unchanged in the elastic regime, indicating no grain rotation during elastic deformation. The onset of change in intensity coincides with the onset of the nonlinearities in Figure 10 and the onset of peak broadening in Figure 11a & b. For both samples, the intensity of 220 reflection decreases during plastic deformation whilst the intensities of 200 and 111 reflections increase. This indicates that the original <110> oriented grains rotate to other orientations, and <100> and <111> oriented grains increases due to the rotation of other oriented grains.

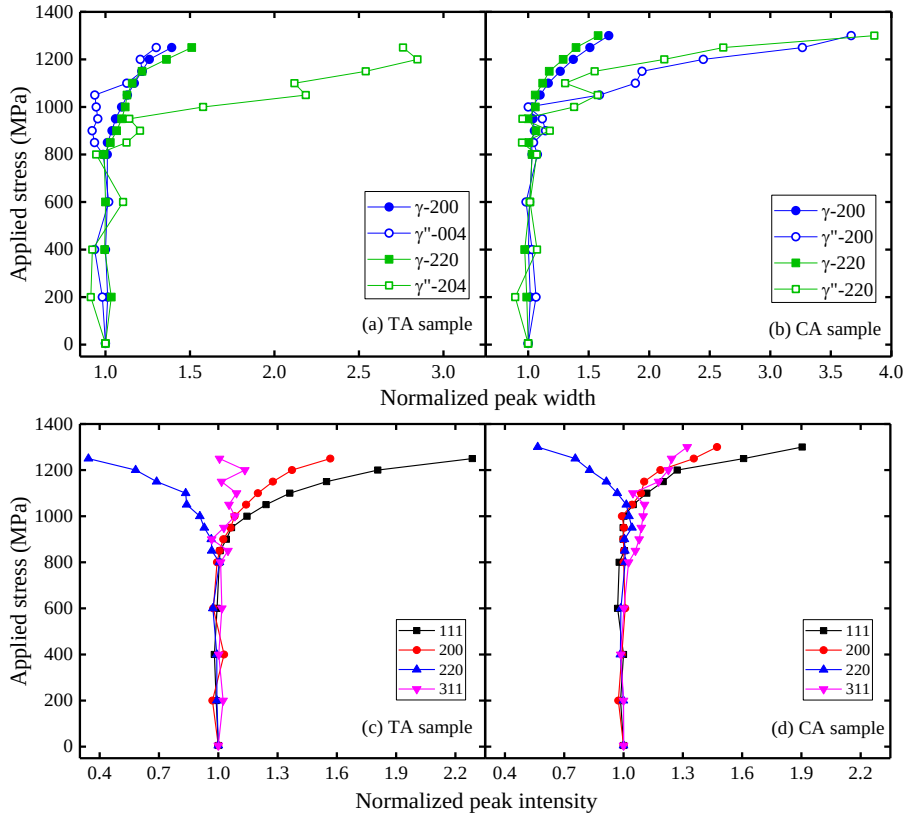

Figure 11. Evolution of normalized peak broadening of the γ and γ″ phases in the {200} and {220} oriented grains for the (a) tensile-aged (TA), (b) compressive-aged (CA) samples. And peak intensity evolution for (c) TA and (d) CA samples. Error bars for peak width associated with uncertainties of peak fitting are about the size of the symbol in the elastic regime, and increase from 0.07 to 0.44 in the plastic regime for both phases. Error bars for peak intensity are about the size of the symbol. Error bars are not shown for clarity.

4. Discussions

4.1. Localised deformation mechanism

Various deformation mechanisms associated with the γ″ precipitate were proposed based on TEM observations or simulations: dislocation shearing (anti-phase boundary (APB) shearing, stacking fault (SF) shearing, micro-twinning shearing, etc.), and Orowan looping [8–10,12–14]. Some of these deformation mechanisms may be active during deformation at different stages or in different γ″ variants. For example, Sundararaman et al. [9] observed dislocations that associated with APB shearing and SF shearing in samples subjected to small deformation (2% plastic strain) and micro-twinning shearing in samples with large plastic deformation. A combination of *ab initio* calculation and phase field simulation by Lv et al. [13] discovered a partial dislocation loop can be left around the precipitate belonging to certain variants sheared by dislocations.

Although the detailed interactions between dislocations and precipitates cannot be revealed by neutron diffraction, lattice strain response to the applied stress during deformation can act as a trace of the predominant deformation behaviour: (1) when dislocations from the matrix enter the precipitate and cut through it, the precipitate and the matrix deform jointly and would not carry extra loads. As a result, both phases accumulate little increase in lattice strain with increasing stress. This is the case for the <110> oriented grains in the two samples at the early stage of plastic deformation, during which the lattice strain of both phases goes straight up (green plots in Figure 10a & b). Meanwhile, loads transfer from the yielding grains to those unyielded grains, i.e. <100> oriented grains, as shown in blue plots in Figure 10a & b that experienced accelerated lattice strain accumulation. (2) With further deformation, dislocation shearing the precipitates becomes more difficult whilst dislocation bypassing becomes the dominant process of deformation. When this happens, loads transfer from the matrix to the γ" phase, as observed from the green plots in Figure 10a & b at larger plastic deformation when the γ" phase accumulates larger lattice strain than the matrix phase. The transition from shearing to bypassing is yet unclear. Two possible mechanisms can be the candidates to account for the transition: a). although the shearing mechanism is predominant at the early stage, bypassing can be operating at the same time to a less extent given that the critical resolved shear stress (CRSSs) for each deformation mode are not in much difference and vary depending on precipitate size. The left behind dislocation loops by bypassing accumulate and make the shearing become more difficult and the transition can happens.

b). According to Lv et al. [13], dislocation shearing can leave partial dislocation loops around precipitate. These partial dislocation loops can hinder the following dislocation from entering the sheared precipitate and bypassing becomes more favourite. (3) The lattice strain of both phases in the <100> oriented grains of the TA sample displays accelerated accumulation during plastic deformation until failure (blue square plots in Figure 10a), indicating that both phases in these grains carry extra loads transferred from those yielded grains but preserve elastically deformed. This is also evident from the small peak broadening of the two phases shown in Figure 11a. In contrast, the lattice strain evolution of the two phases in the CA sample differs from each other at the onset of yielding (blue plots in Figure 10b) accompanied by large peak broadening of the γ" phase (Figure 11b), suggesting the γ" phase is being yielded while the matrix remains unyielded in the <100> oriented grains. This acts as a sign of microtwinning that confined in the γ" precipitates yet not propagate into the matrix. Intrinsic stacking faults can be common in large γ" precipitates due to an ultralow energy (~2.3 mJ/m^2) [13,43] and serve as a precursor of microtwinning [13]. Indeed, microtwinning has been reported as the deformation mechanism by Sundararaman *et al*. [9] from their observations of a great majority of such microtwins in γ" and an estimation of a lower CRSS than that for either dislocation shear or bypassing mechanisms. In addition, McAllister *et al*. [14] also observed microtwinning as a prominent deformation mode at elevated temperatures in commercially aged IN718. Both studies revealed that the micro twins are conserved in the γ" but not extended into the matrix. It is interesting to note from the lattice strain evolution that the micro twinning occurs in the <100> oriented grains where the disk plane of γ" is parallel to the applied stress (Figure 10b), yet not happens in those γ" with disk plane normal to the applied stress (Figure 10a). The underlying mechanism related to the different behaviour remains unknow and worth a further investigation.

The current work focuses on using the *in situ* neutron diffraction to reveal the deformation behaviour during tensile deformation in a relatively large gauge volume. Attempts to obtain dislocation structure micrographs via transmission electron microscopy (TEM) on the fractured samples were not successful. Challenges come from the very high dislocation density in the fractured samples as well as the multi-mechanisms happened during deformation, micrographs showing vast dislocations does not help to unravel the micro-mechanism in a conclusive way. One way to tackle this would be to obtain micrographs on tensile samples interrupted at different plastic strains. In addition, crystallographic orientation of the TEM foils with respect to the loading direction has to

be carefully selected to reflect the grain specific deformation behaviour. Nevertheless, the lattice strain evolution of both the matrix and precipitate phases bridges the gap between the micro and macro scale of deformation behaviour in a more representative manner thanks to the large gauge volume scanned and the grains and phases selective characteristic.

4.2. γ″ variant-sensitive strengthening

It is shown in Section 3.4 that the yield strength of the CA sample is greater than that of the TA sample. Despite microstructures show that the former possesses a slightly larger grain size, the major difference remains in the different γ″ variant distributions, which is the most likely reason accounting for the different level of strengthening. Indeed, substantial studies have pointed out that the interaction between dislocations and γ″ precipitates is variant-dependent, although the detailed underlying mechanisms vary. In early studies by Oblak *et al*. [8] and Chaturvedi *et al*. [10], they observed pairs and/or quadruplets of 1/2<110> dislocations, which interact with variants differently. A recent study using scanning transmission electron microscopy found no evidence of such pairs or quadruplets 1/2<110> dislocations but the existence of 1/6<112> dislocations [12]. Phase field simulation by the same group showed the 1/6<112> dislocations, which are a result of 1/2<110> dislocation pair with different burgers vectors (i.e. 1/2[110] and 1/2[101]), are more likely the operative dislocations that shear the three variants uniquely [12–14], although the simulation did not take the coherency stress of the precipitates into account.

An estimation of the CRSS increment with variant dependence based on coherency strengthening was developed by Oblak *et al*. [7]. According to the coherency strengthening mechanism, the misfit stress fields that arise from the large tetragonal lattice misfit between the γ″ and γ will interact with dislocations [44]. The stress field of an ellipsoid is rather complex, making the description of interaction between dislocations and particle stress field difficult. Oblak *et al*. [7] simplified the problem assuming the dislocation is a straight line that has an average stress at the centre of the particle. Considering the γ″ phase whose misfit is tetragonal, there is a major strain axis (which is parallel to its c-axis), and minor strain axes (along which the strain can be neglected), an active dislocation does not interact equally with all the three γ″ variants. Instead, a stronger interaction occurs when the angle between the Burgers vector of a dislocation and the strain axis of the precipitate is smaller, and vice versa. The estimation successfully

matched the experimental difference in CRSS increment between samples with different variant distributions [8], which were IN718 in single crystal form and aged with either a tensile or compressive stress along its [001] direction in a similar way to this study.

It is worthy to point out that the CRSS increment in the TA and CA samples in the form of single crystal is opposite to our findings, which is the TA single crystal sample gained a larger CRSS increment than the compressive one. The different findings between polycrystal (this study) and single crystal [8] can be attributed to their different active slip systems. In fact, the CRSS increment in the current study can be explained using Oblak's equation, which will be shown in follows.

Figure 12 schematically illustrates the active slip systems with different Burgers vectors and γ″ precipitates in the grain oriented with [011] parallel to the loading direction. Note that for the TA sample, Figure 12a shows the presence of only the [001] and [010] γ″ variants whose c-axis is 45° to the applied load. Conversely, for the CA sample, Figure 12b shows the presence of only the [100] γ″ variant whose c-axis is 90° to the applied load. The four active slip systems, whose Schmid factors are the largest among the twelve slip systems, with different Burgers vectors are shown. For the TA sample, when the dislocations approach the γ″ precipitates, the dislocations whose Burgers vectors are **b**=1/2[-101] and **b**=1/2[101] will have strong interactions with the [001] variant and weak interactions with the [010] variant, the reason is that their Burgers vectors are at 45° to the major strain axis of the [001] variant and at 90° to the [010] variant. For the interaction between dislocations of the other two slip systems and precipitates, the strong / weak interactions swap for the same reason. In contrast, for the CA sample (Figure 12b), dislocations of all the four slip systems will have strong interactions with the [100] variant since the Burgers vectors are all at 45° to the major axis of the precipitate. In other words, the dislocation / precipitate interaction 'efficiency' is doubled in the CA <110> oriented grains compared to the TA <110> oriented grains, contributing to a larger increment in the CRSS in the CA sample than the TA sample.

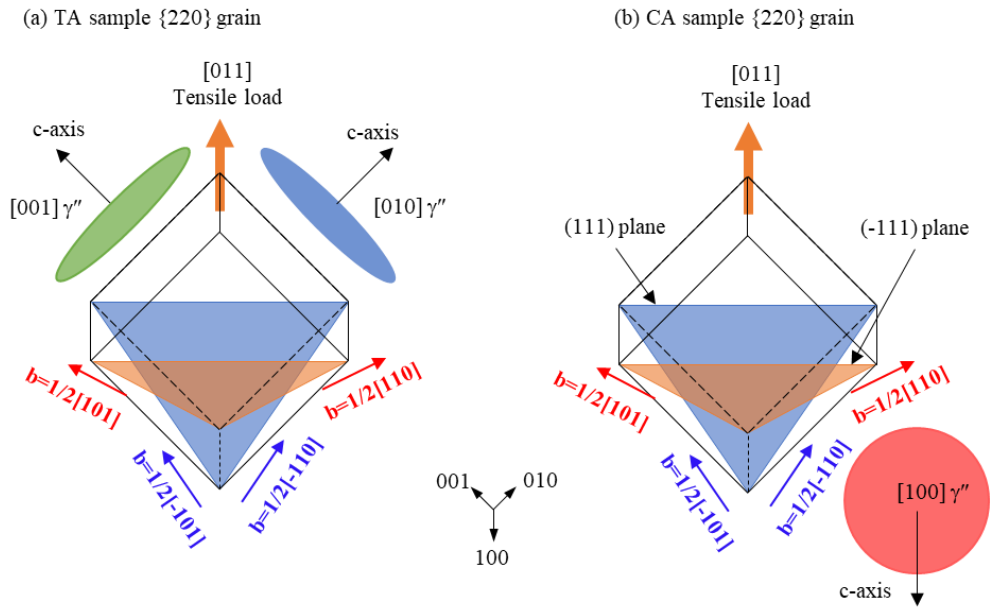

Figure 12. Schematic illustrations of active dislocations (arrows in blue and red) and existing γ″ variants in grains oriented with [011] parallel to loading direction in the (a) tensile-aged (TA) sample, and (b) compressive-aged (CA) sample.

According to the coherency strain strengthening mechanism, the increment in CRSS arises from dislocation shearing the γ″ particle is given by [8]

$$\Delta\tau = 1.7G|\varepsilon|^{3/2}\left[\frac{h^2 f\beta}{2bR}\right]^{\frac{1}{2}} \quad (3)$$

, where G is the shear modulus of γ matrix, ε is the stress free transformation strain along the normal of the γ″ precipitate, b is the magnitude of Burgers vector of the dislocation shearing the γ″ precipitates, f is the volume fraction of the γ″ precipitates, R is the half of the major axis of the γ″ precipitates, h is the half thickness of the ellipsoidal, $\beta = 1/2$ for the half interaction efficiency in the TA <110> oriented grains where 2 variants present, or $\beta = 1$ for the full interaction efficiency in the CA <110> oriented grains where only 1 variant presents. The ε, R and h have been measured and reported in our previous study [31]. The f is derived from the intensity of {220} γ peak and {204} γ″ peak from neutron diffraction of the TA sample with scattering structure factor taken into account:

$$\frac{I^{\gamma''}}{I^{\gamma''}} = \frac{(\lambda^{\gamma''})^3(\eta_{\gamma''})^2 f_{\gamma''}}{(\lambda^{\gamma})^3(\eta_{\gamma})^2 f_{\gamma}} \quad (4)$$

, where I is the intensity, λ is the wavelength of diffraction neutron beam, η the scattering density, the detailed calculation is referred to a previous study in ref. [30]. The G and b are adopted from reference [8]. The parameters for the calculation are listed in Table 5.

Table 5. Parameters for the calculation of CRSS increment.

G [8]	b [8]	f [30]	ε [31]	R [31]	h [31]	β
70 GPa	0.254 nm	0.08	0.031	28 nm	6.1nm	½ or 1

The increment in CRSS for the TA and CA samples were calculated to be $\Delta\tau_T = 213$ MPa and $\Delta\tau_C = 301$ MPa, respectively. The difference in $\Delta\tau$ of the two samples is $\Delta\tau_C - \Delta\tau_T = 88$ MPa, considering the Schmid factor $m = 0.408$ for these active slip systems, the difference in yield strength is $\Delta\sigma_{yield} = \frac{\Delta\tau_C - \Delta\tau_T}{m} = 216$ MPa. This calculated value is larger than the experimental difference (110 MPa from Table 4) by 96%. The discrepancy could be due to that the extent of variant selection was not that complete in the <110> oriented grains. Evidence can be found with a careful observation of Figure 3d & h, in which a very small portion of the residual variants can be found. In fact, the degree of variant selection is a function of ageing temperature, ageing time, stress applied and grain orientation [16]. Therefore, the β is probably slightly larger than ½ for the TA sample and smaller than 1 for the CA one. With $\beta = 0.6$ for the former and $\beta = 0.9$ for the latter, a value of $\Delta\sigma_{\text{yield}} = 129$ MPa is achieved, which agrees well with the experimental value.

Mechanical property is highly dependent on microstructure which is an outcome of the thermomechanical history. Among the sophisticated microstructures, the variant distributions have a direct effect on the coherency strengthening. The variant-dependent effect brings several implications. If such an alloy were aged under a high level of stress, which could happen in additively manufactured IN718 part where localized residual stresses can be very large, the γ″ variant distribution could be profoundly inhomogeneous, resulting in an unexpected mechanical performance. On the other hand, mechanical performance can be improved with deliberately tailoring the γ″ variant distribution, i.e. direct ageing of cold-rolled IN718, during which process high level of residual stresses are induced [17].

5. Summary

This study reports the deformation behaviour related to the γ″ strengthening phase of IN718 *in situ* for the first time. This *in situ* neutron diffraction work bridges the grain- and phase-specific micro-mechanisms and macro deformation behaviour via sampling a relatively large gauge volume which is highly representative. In addition, the effect of the

specific γ″ variant on the yield strength is studied via the coherency strengthening theory. The findings of this study are categorized as follows:

i. The *hkl*-specific Diffraction elastic constants (DECs) of the γ″ phase were measured. It is shown the γ″ phase is stiffer along its c-axis than along its a-axis.

ii. From the point of view of the stress-lattice strain evolution and diffraction peak width evolution, the plastic deformation first takes place in the grains oriented with <110> parallel to the loading direction as the γ matrix and the γ″ precipitates are jointly deformed, which can be attributed to dislocations shearing precipitates process at the early stage of plastic deformation. At the later stage, the deformation by dislocations bypassing the γ″ precipitates become predominant. In addition, occurrence of microtwinning is suggested by the lattice strain deviation in the <100> oriented grains of the compressive-aged sample.

iii. The compressive-aged samples display a larger yield strength compared to the tensile-aged sample. Analysis combining the coherency strengthening model and variant distributions in the two samples reveals that dislocation-precipitate interaction in the compressive-aged sample is more effective compared to that in the tensile-aged sample. The calculated variation in yield strength agrees with the experimental value, indicating the variant-sensitive dislocation-precipitate interaction accounts for the variation in strengthening.

Acknowledgements

Ruiyao Zhang gratefully acknowledges the support by Guangdong Introducing Innovative and Entrepreneurial Teams (2016ZT06G025), and the financial support from the Centre for Doctoral Training in Innovative Metal Processing (IMPaCT) funded by the UK Engineering and Physical Sciences Research Council (EPSRC), grant reference EP/L016206/1. The authors also acknowledge useful discussions by Dr. Xingzhong Liang, and the allocation of beam time (RB1820207) at ENGIN-X, ISIS, Rutherford Appleton Laboratory. Chinnapat Panwisawas would like to acknowledge the funding from Innovation Fellowship by EPSRC, UK Research and Innovation (UKRI), under the grant

number: EP/S000828/2. Shuyan Zhang gratefully acknowledges the support by Guangdong Major Project of Basic and Applied Basic Research (No. 2020B0301030001), and by the Strategic Priority Research Program of the Chinese Academy of Sciences, Grant No. XDC04000000.

References

[1] R.C. Reed, The superalloys: fundamentals and applications, 1st., Cambridge University Press, Cambridge, 2006.

[2] M.J. Donachie, S.J. Donachie, Superalloys: A Technical Guide Second Edition, ASM International, Materials Park, US, 2002. http://site.ebrary.com/lib/leicester/docDetail.action?docID=10320374.

[3] Y.-L. Kuo, A. Kamigaichi, K. Kakehi, Characterization of Ni-Based Superalloy Built by Selective Laser Melting and Electron Beam Melting, Metall. Mater. Trans. A. 49 (2018) 3831–3837. https://doi.org/10.1007/s11661-018-4769-y.

[4] S.S. Babu, N. Raghavan, J. Raplee, S.J. Foster, C. Frederick, M. Haines, R. Dinwiddie, M.K. Kirka, A. Plotkowski, Y. Lee, R.R. Dehoff, Additive Manufacturing of Nickel Superalloys: Opportunities for Innovation and Challenges Related to Qualification, Metall. Mater. Trans. A. 49 (2018) 3764–3780. https://doi.org/10.1007/s11661-018-4702-4.

[5] H.Y. Wan, Z.J. Zhou, C.P. Li, G.F. Chen, G.P. Zhang, Effect of scanning strategy on grain structure and crystallographic texture of Inconel 718 processed by selective laser melting, J. Mater. Sci. Technol. 34 (2018) 1799–1804. https://doi.org/https://doi.org/10.1016/j.jmst.2018.02.002.

[6] H. Yang, G. Jing, P. Gao, Z. Wang, X. Li, Effects of circular beam oscillation technique on formability and solidification behaviour of selective laser melted Inconel 718: From single tracks to cuboid samples, J. Mater. Sci. Technol. 51 (2020) 137–150. https://doi.org/https://doi.org/10.1016/j.jmst.2019.09.044.

[7] J.M. Oblak, D.S. Duvall, D.F. Paulonis, An estimate of the strengthening arising from coherent, tetragonally-distorted particles, Mater. Sci. Eng. 13 (1974) 51–56. https://doi.org/https://doi.org/10.1016/0025-5416(74)90020-2.

[8] J.M. Oblak, D.F. Paulonis, D.S. Duvall, Coherency strengthening in Ni base alloys hardened by D022 γ″ precipitates, Metall. Trans. 5 (1974) 143. https://doi.org/10.1007/bf02642938.

[9] M. Sundararaman, P. Mukhopadhyay, S. Banerjee, Deformation behaviour of γ″ strengthened inconel 718, Acta Metall. 36 (1988) 847–864. https://doi.org/http://dx.doi.org/10.1016/0001-6160(88)90139-3.

[10] M.C. Chaturvedi, Y.F. Han, Strengthening mechanisms in Inconel 718 superalloy, Met. Sci. 17 (1983) 145–149. https://doi.org/10.1179/030634583790421032.

[11] N. Zhou, D.C. Lv, H.L. Zhang, D. McAllister, F. Zhang, M.J. Mills, Y. Wang, Computer simulation of phase transformation and plastic deformation in IN718 superalloy: Microstructural evolution during precipitation, Acta Mater. 65 (2014) 270–286. https://doi.org/10.1016/j.actamat.2013.10.069.

[12] D. McAllister, D. Lv, B. Peterson, H. Deutchman, Y. Wang, M.J. Mills, Lower temperature deformation mechanisms in a γ″-strengthened Ni-base superalloy, Scr. Mater. 115 (2016) 108–112. https://doi.org/https://doi.org/10.1016/j.scriptamat.2015.11.026.

[13] D.C. Lv, D. McAllister, M.J. Mills, Y. Wang, Deformation mechanisms of D022 ordered intermetallic phase in superalloys, Acta Mater. 118 (2016) 350–361. https://doi.org/10.1016/j.actamat.2016.07.055.
[14] D. McAllister, D. Lv, L. Feng, H. Deutchman, A. Wessman, Y. Wang, M.J. Mills, Characterization and Modeling of Deformation Mechanisms in Ni-Base Superalloy 718 BT - Proceedings of the 9th International Symposium on Superalloy 718 & Derivatives: Energy, Aerospace, and Industrial Applications, in: E. Ott, X. Liu, J. Andersson, Z. Bi, K. Bockenstedt, I. Dempster, J. Groh, K. Heck, P. Jablonski, M. Kaplan, D. Nagahama, C. Sudbrack (Eds.), Springer International Publishing, Cham, 2018: pp. 319–338.
[15] H. Qin, Z. Bi, H. Yu, G. Feng, R. Zhang, X. Guo, H. Chi, J. Du, J. Zhang, Assessment of the stress-oriented precipitation hardening designed by interior residual stress during ageing in IN718 superalloy, Mater. Sci. Eng. A. 728 (2018) 183–195. https://doi.org/https://doi.org/10.1016/j.msea.2018.05.016.
[16] H. Qin, Z. Bi, R. Zhang, T.L. Lee, H. Yu, H. Chi, D. Li, H. Dong, J. Du, J. Zhang, Stress-Induced Variant Selection of γ″ Phase in Inconel 718 During Service: Mechanism and Effects on Mechanical Behavior BT - Superalloys 2020, in: S. Tin, M. Hardy, J. Clews, J. Cormier, Q. Feng, J. Marcin, C. O'Brien, A. Suzuki (Eds.), Springer International Publishing, Cham, 2020: pp. 713–725. https://doi.org/https://doi.org/10.1007/978-3-030-51834-9_69.
[17] H. Zhang, C. Li, Q. Guo, Z. Ma, H. Li, Y. Liu, Improving creep resistance of nickel-based superalloy Inconel 718 by tailoring gamma double prime variants, Scr. Mater. 164 (2019) 66–70. https://doi.org/https://doi.org/10.1016/j.scriptamat.2019.01.041.
[18] Q. Zhu, G. Chen, C. Wang, L. Cheng, H. Qin, P. Zhang, Microstructure evolution and mechanical property characterization of a nickel-based superalloy at the mesoscopic scale, J. Mater. Sci. Technol. 47 (2020) 177–189. https://doi.org/https://doi.org/10.1016/j.jmst.2020.02.021.
[19] S. Huang, Y. Gao, K. An, L. Zheng, W. Wu, Z. Teng, P.K. Liaw, Deformation mechanisms in a precipitation-strengthened ferritic superalloy revealed by in situ neutron diffraction studies at elevated temperatures, Acta Mater. 83 (2015) 137–148. https://doi.org/https://doi.org/10.1016/j.actamat.2014.09.053.
[20] B.M.B. Grant, E.M. Francis, J.Q. da Fonseca, M.R. Daymond, M. Preuss, Deformation behaviour of an advanced nickel-based superalloy studied by neutron diffraction and electron microscopy, Acta Mater. 60 (2012) 6829–6841. https://doi.org/http://dx.doi.org/10.1016/j.actamat.2012.09.005.
[21] D. Dye, H.J. Stone, R.C. Reed, A two phase elastic–plastic self-consistent model for the accumulation of microstrains in Waspaloy, Acta Mater. 49 (2001) 1271–1283. https://doi.org/http://dx.doi.org/10.1016/S1359-6454(01)00003-9.
[22] H.J. Stone, T.M. Holden, R.C. Reed, On the generation of microstrains during the plastic deformation of Waspaloy, Acta Mater. 47 (1999) 4435–4448. https://doi.org/http://dx.doi.org/10.1016/S1359-6454(99)00314-6.
[23] B. Clausen, T. Lorentzen, M.A.M. Bourke, M.R. Daymond, Lattice strain evolution during uniaxial tensile loading of stainless steel, Mater. Sci. Eng. A. 259 (1999) 17–24. https://doi.org/https://doi.org/10.1016/S0921-5093(98)00878-8.
[24] B. Clausen, T. Lorentzen, T. Leffers, Self-consistent modelling of the plastic deformation of f.c.c. polycrystals and its implications for diffraction measurements of internal stresses, Acta Mater. 46 (1998) 3087–3098. https://doi.org/https://doi.org/10.1016/S1359-6454(98)00014-7.
[25] B. Clausen, T. Lorentzen, Experimental evaluation of a polycrystal deformation modeling scheme using neutron diffraction measurements, Metall. Mater. Trans. A. 28 (1997) 2537–2541. https://doi.org/10.1007/s11661-997-0011-z.
[26] J. Cormier, P. Gadaud, M. Czaplicki, R.Y. Zhang, H.B. Dong, T.M. Smith, F. Zhang, J.S. Tiley, S.L. Semiatin, In-Situ Determination of Precipitation Kinetics During Heat Treatment of Superalloy 718, Metall. Mater. Trans. A. (2020). https://doi.org/10.1007/s11661-020-06078-4.

[27] S.L. Semiatin, J.S. Tiley, F. Zhang, T.M. Smith, R.Y. Zhang, H.B. Dong, P. Gadaud, J. Cormier, A Fast-Acting Method for Simulating Precipitation During Heat Treatment of Superalloy 718, Metall. Mater. Trans. A. 52 (2021) 483–499. https://doi.org/10.1007/s11661-020-06092-6.
[28] H. Li, G. Sun, W. Woo, J. Gong, B. Chen, Y. Wang, Y.Q. Fu, C. Huang, L. Xie, S. Peng, Tensile deformation behaviors of Zircaloy-4 alloy at ambient and elevated temperatures: In situ neutron diffraction and simulation study, J. Nucl. Mater. 446 (2014) 134–141. https://doi.org/https://doi.org/10.1016/j.jnucmat.2013.12.006.
[29] E.-W. Huang, R.I. Barabash, Y. Wang, B. Clausen, L. Li, P.K. Liaw, G.E. Ice, Y. Ren, H. Choo, L.M. Pike, D.L. Klarstrom, Plastic behavior of a nickel-based alloy under monotonic-tension and low-cycle-fatigue loading, Int. J. Plast. 24 (2008) 1440–1456. https://doi.org/https://doi.org/10.1016/j.ijplas.2007.10.001.
[30] R.Y. Zhang, H.L. Qin, Z.N. Bi, J. Li, S. Paul, T.L. Lee, B. Nenchev, J. Zhang, S. Kabra, J.F. Kelleher, H.B. Dong, Using Variant Selection to Facilitate Accurate Fitting of γ″ Peaks in Neutron Diffraction, Metall. Mater. Trans. A. 50 (2019) 5421–5432. https://doi.org/10.1007/s11661-019-05393-9.
[31] R.Y. Zhang, H.L. Qin, Z.N. Bi, J. Li, S. Paul, T.L. Lee, S.Y. Zhang, J. Zhang, H.B. Dong, Temperature-Dependent Misfit Stress in Gamma Double Prime Strengthened Ni-Base Superalloys, Metall. Mater. Trans. A. (2020). https://doi.org/10.1007/s11661-020-05627-1.
[32] R.Y. Zhang, H.L. Qin, Z.N. Bi, J. Li, S. Paul, T.L. Lee, S.Y. Zhang, J. Zhang, H.B. Dong, Evolution of Lattice Spacing of Gamma Double Prime Precipitates During Aging of Polycrystalline Ni-Base Superalloys: An In Situ Investigation, Metall. Mater. Trans. A. (2019). https://doi.org/10.1007/s11661-019-05536-y.
[33] W.F. Hosford, S.P. Agrawal, Effect of stress during aging on the precipitation of θ′ in Al-4 Wt pct Cu, Metall. Trans. A. 6 (1975) 487. https://doi.org/10.1007/bf02658406.
[34] A. Pineau, Influence of uniaxial stress on the morphology of coherent precipitates during coarsening—elastic energy considerations, Acta Metall. 24 (1976) 559–564. https://doi.org/https://doi.org/10.1016/0001-6160(76)90101-2.
[35] M. Gao, D.G. Harlow, R.P. Wei, S. Chen, Preferential coarsening of γ″ precipitates in INCONEL 718 during creep, Metall. Mater. Trans. A. 27 (1996) 3391–3398. https://doi.org/10.1007/bf02595432.
[36] D.Y. Li, L.Q. Chen, Selective variant growth of coherent Ti11Ni14 precipitate in a TiNi alloy under applied stresses, Acta Mater. 45 (1997) 471–479. https://doi.org/https://doi.org/10.1016/S1359-6454(96)00207-8.
[37] J.R. Santisteban, M.R. Daymond, J.A. James, L. Edwards, ENGIN-X: a third-generation neutron strain scanner, J. Appl. Crystallogr. 39 (2006) 812–825.
[38] K. Kulawik, P.A. Buffat, A. Kruk, A.M. Wusatowska-Sarnek, A. Czyrska-Filemonowicz, Imaging and characterization of γ′ and γ″ nanoparticles in Inconel 718 by EDX elemental mapping and FIB–SEM tomography, Mater. Charact. 100 (2015) 74–80. https://doi.org/10.1016/j.matchar.2014.12.012.
[39] R.B. Li, M. Yao, W.C. Liu, X.C. He, Isolation and determination for δ, γ′ and γ″ phases in Inconel 718 alloy, Scr. Mater. 46 (2002) 635–638. https://doi.org/http://dx.doi.org/10.1016/S1359-6462(02)00041-6.
[40] M.T. Hutchings, P.J. Withers, T.M. Holden, T. Lorentzen, Introduction to the characterization of residual stress by neutron diffraction, Taylor & Francis, Boca Raton, Fla., 2005.
[41] D.M. Collins, N. D'Souza, C. Panwisawas, In-situ neutron diffraction during stress relaxation of a single crystal nickel-base superalloy, Scr. Mater. 131 (2017) 103–107. https://doi.org/10.1016/j.scriptamat.2017.01.002.
[42] N. D'Souza, J. Kelleher, C. Qiu, S.-Y. Zhang, S. Gardner, R.E. Jones, D. Putman, C. Panwisawas, The role of stress relaxation and creep during high temperature deformation in Ni-base single crystal superalloys – Implications to strain build-up during directional solidification, Acta Mater. 106 (2016) 322–332. https://doi.org/http://dx.doi.org/10.1016/j.actamat.2016.01.032.

[43] A. Niang, J. Huez, J. Lacaze, B. Viguier, Characterizing Precipitation Defects in Nickel Based 718 Alloy, Mater. Sci. Forum. 636–637 (2010) 517–522. https://doi.org/10.4028/www.scientific.net/MSF.636-637.517.
[44] V. Gerold, H. Haberkorn, On the Critical Resolved Shear Stress of Solid Solutions Containing Coherent Precipitates, Phys. Status Solidi. 16 (1966) 675–684. https://doi.org/10.1002/pssb.19660160234.

γ″ variant-sensitive deformation behaviour of Inconel 718 superalloy

R.Y. Zhang [a, b, 1, *], H.L. Qin [c, 1], Z.N. Bi [c], Y.T. Tang [d], J. Araújo de Oliveira [e], T.L. Lee [f], C. Panwisawas [b], S.Y. Zhang [a], J. Zhang [c], J. Li [g], H.B. Dong [b, *]

[a] *Centre of Excellence for Advanced Materials, Dongguan, 523808, China*

[b] *School of Engineering, University of Leicester, University Road, Leicester LE1 7RH, UK*

[c] *Beijing Key Laboratory of Advanced High Temperature Materials, Central Iron and Steel Research Institute, No. 76 Xueyuannanlu, Haidian, Beijing, 100081, China*

[d] *Department of Materials, University of Oxford, Parks Road, Oxford OX1 3PH, United Kingdom*

[e] *StressMap, Engineering and Innovation Department, The Open University, Walton Hall, Milton Keynes MK7 6AA, UK*

[f] *ISIS Neutron Source, Rutherford Appleton Laboratory, Harwell Science and Innovation Campus, Chilton, Oxfordshire, OX11 0QX, UK*

[g] *School of Material Science and Engineering, Shanghai Jiao Tong University, Shanghai, 200240, China*

[1] These authors contributed equally to this work and should be considered co-first authors: R.Y. Zhang, H.L. Qin

* Corresponding authors: (R.Y. Zhang) Email address: ruiyao.zhang@ceamat.com, (H.B. Dong) Tel: +44 116 2522528, Email address: hd38@le.ac.uk

H.B. Dong
Professor of Materials Engineering
Research Chair of Royal Academy of Engineering
Director of EPSRC CDT in Innovative Metal Processing
School of Engineering
University of Leicester
University Road, Leicester
LE1 7RH, UK
Tel:+44 116 2522528
Email: h.dong@le.ac.uk

17, Dec. 2021

Editor
Journal of materials science and technology

Cover letter

Dear Editor,

Please find attached our manuscript entitled "γ″ variant-sensitive deformation behaviour of Inconel 718 superalloy", by R.Y. Zhang et al., which we would like to submit for publication as a research paper in Journal of materials science and technology.

In this paper we report the deformation behaviour of both the γ matrix and different variants of the γ″ precipitates in Inconel 718 superalloy during tensile deformation. Based on the neutron diffraction data and microstructure observation, it is revealed that the γ matrix and γ″ precipitates are jointly deformed at the early stage of plastic deformation, suggesting that dislocation shearing the γ″ precipitates occurs at this stage. It is also found that the increments in strengthening are different for samples with different γ″ variant distribution, the different strengthening is believed to be attributed to the different efficiency of interactions between active dislocations and different variants.

In this study, two Inconel 718 bar samples were prepared by ageing heat treatment with either a tensile or compressive stress of 300 MPa applied respectively. The purpose of the applied stress during ageing was to form the different γ″ variant distributions in the two samples. These two samples were then subjected to *in situ* tensile deformation neutron diffraction experiment at room temperature. Stress-lattice strain curves for both the γ and γ″ phases were successfully interpreted from the neutron data. It is shown that, during plastic deformation, the γ and γ″ were jointly deformed by dislocation shearing in {220} oriented grains regardless the different variant distributions. However, the different variant distributions has contributed varied level of strengthening, which can be attributed to the different interactions between dislocations and different γ″ variant. Calculated increments in critical resolved shear stress agree well with the differences in measured values.

This study reveals the micro-mechanism of deformation behaviour of Inconel 718 associated with the different γ″ variants. The findings will be helpful to improve prediction of the mechanical properties of the superalloys with the γ″ variant distribution being considered. Examples include those components manufactured either via conventional method or 3D printing that experience intense thermomechanical history.

This manuscript has not been published anywhere else and is not under consideration by another journal. All authors have approved the manuscript and agree with submission, and no conflicts of interest to address.

Thank you for your consideration.

Sincerely,

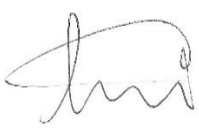

H.B. Dong (Corresponding author)

declaration of conflict interest

Declaration of interests

☒ The authors declare that they have no known competing financial interests or personal relationships that could have appeared to influence the work reported in this paper.

☐The authors declare the following financial interests/personal relationships which may be considered as potential competing interests:

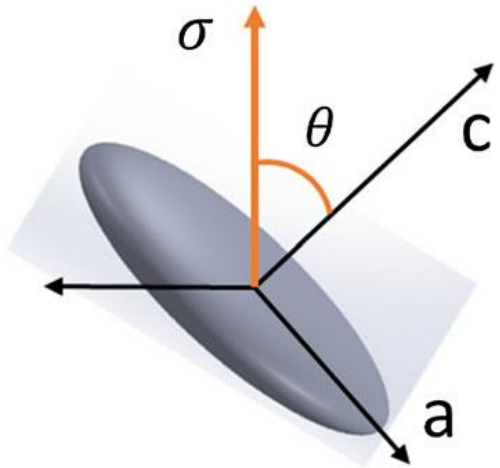

Figure 1. An illustration of the angle θ between stress axis and *c-axis* of a γ″ precipitate [30].

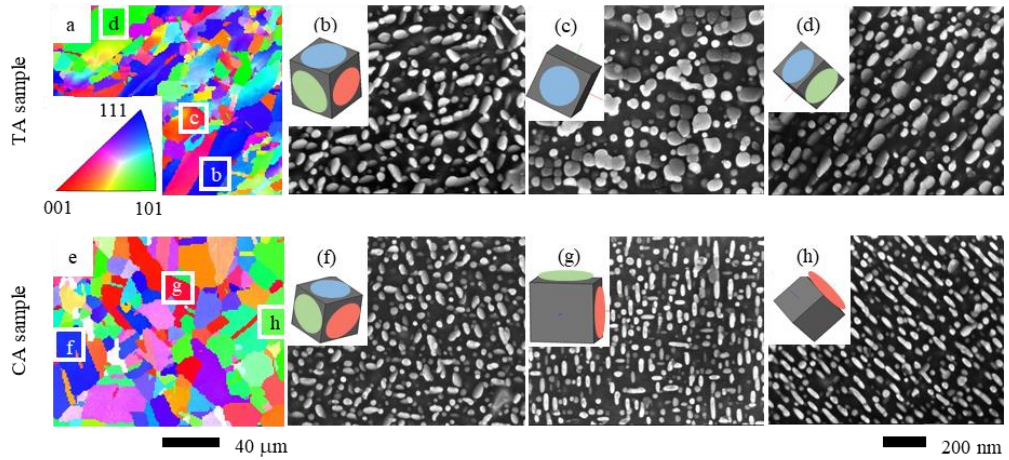

Figure 2. (a) IPF along Z-axis on the cross-section of the TA sample, (b)-(d) γ″ variant distribution in grains selected from locations indicated in (a), (e) IPF on the cross-section of the CA sample, (f)-(h) γ″ variant distribution in grains selected from locations indicated in (e). Insets show the orientation of existing γ″ variants (indicated as either coloured ellipse or circle) with habit planes lying on different faces of the grey cube according to the {100}γ″//{100}γ and [100]γ″//<100>γ relationship with the matrix phase.

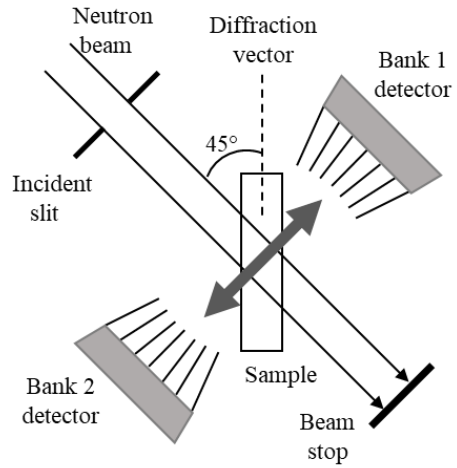

Figure 3. Schematic illustration of in situ neutron diffraction tensile deformation experiment in ENGIN-X, ISIS neutron source, UK.

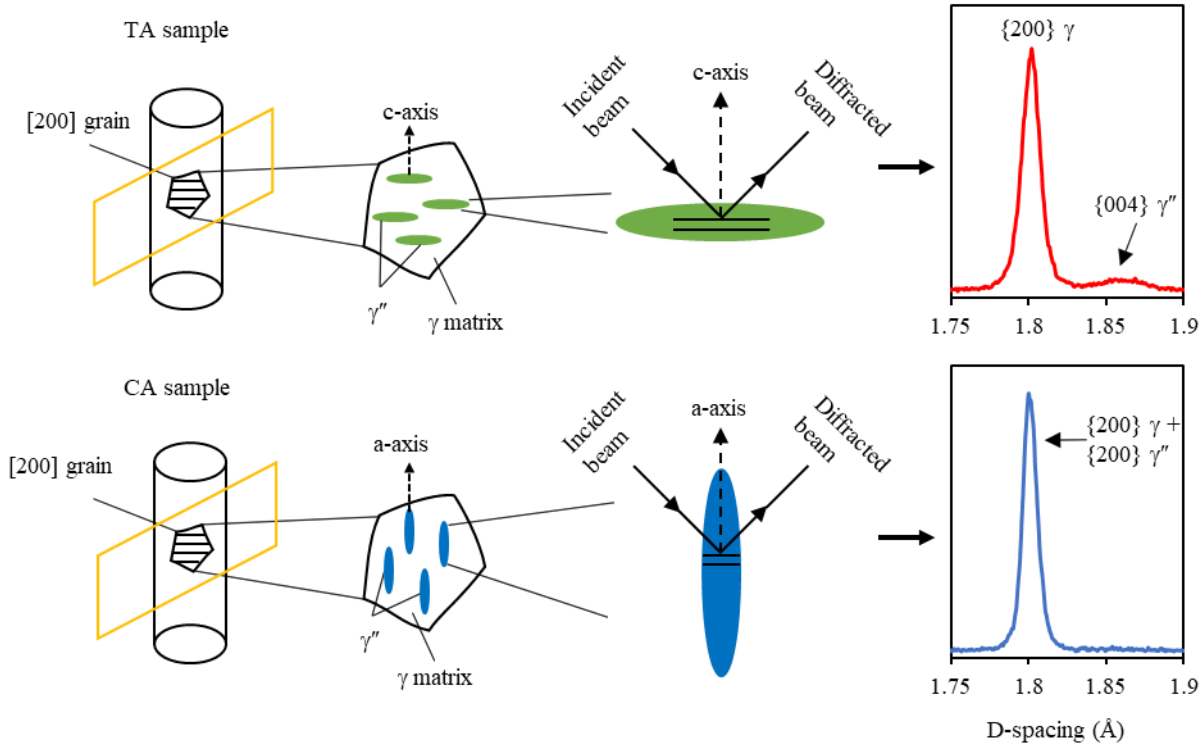

Figure 5. Schematic illustration of diffraction from a <100> oriented grain in (tensile-aged) TA and (compressive-aged) CA samples, respectively, viewing along the transverse direction of the bar sample. Non-overlapping {004} γ" peak are contributed from the variant with c-axis parallel to diffraction vector while the {200} overlapping peak are from the variant with a-axis parallel to the diffraction vector.

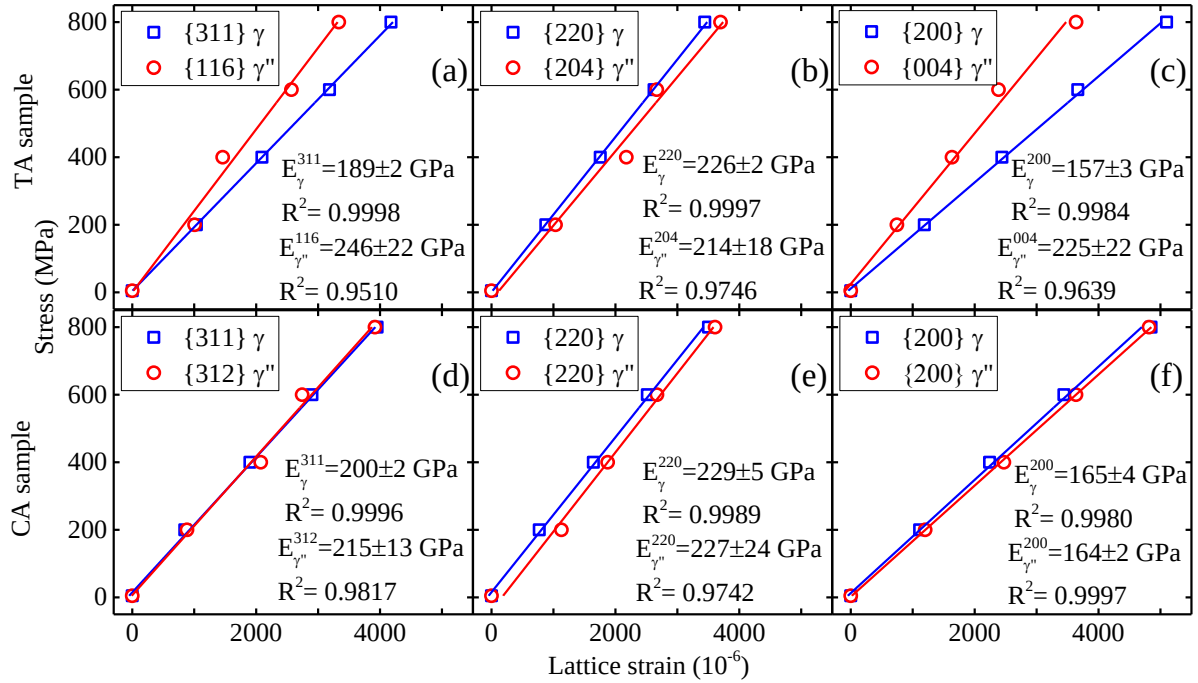

Figure 7. Stress-lattice strain plots for each *hkl* relfection of both the γ and γ″ phases in the elastic regime. (a) – (c) for tensile-aged (TA) sample, (d) – (f) for compressive-aged (CA) sample. Diffraction elastic constants were obtained by linearly fitting to each of the plot. It is shown the γ" is stiffer along its c-axis (<004> direction) than a-axis (<200> direction), as well as stiffer than the matrix phase. Errors bars associated with the fitting uncertainties are about the size of the symbol and not shown for clarity.

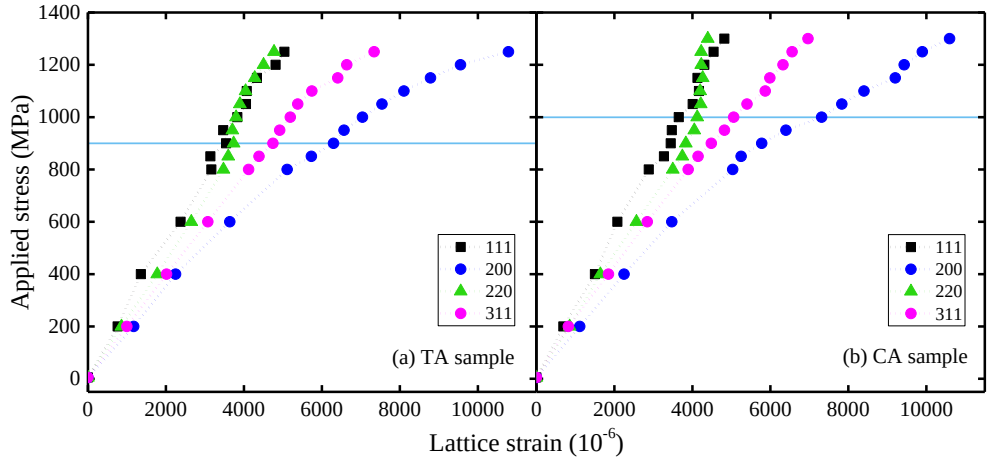

Figure 9. Evolution of *hkl*-specific lattice strain of the γ phase along the longitudinal direction for (a) tensile-aged (TA) and (b) compressive-aged (CA) samples. The horizontal lines indicate the onsets of nonlinearity, which coincide with the 0.2% yield strength obtained from macro stress-strain curves. The error bars associated with uncertainties from peak fitting are about the size of the symbol and not shown here for clarity.

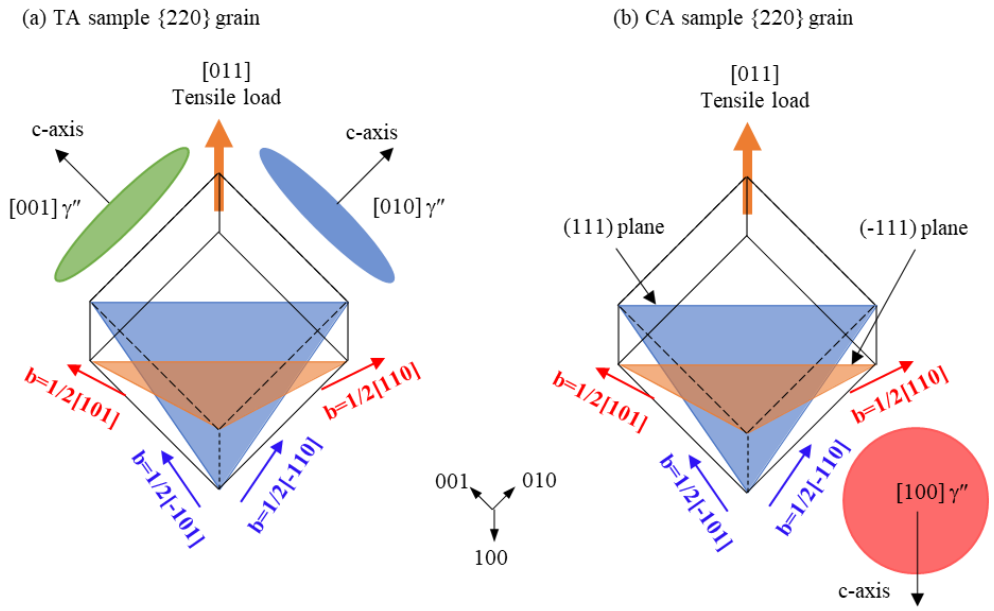

Figure 12. Schematic illustrations of active dislocations (arrows in blue and red) and existing γ″ variants in grains oriented with [011] parallel to loading direction in the (a) tensile-aged (TA) sample, and (b) compressive-aged (CA) sample.

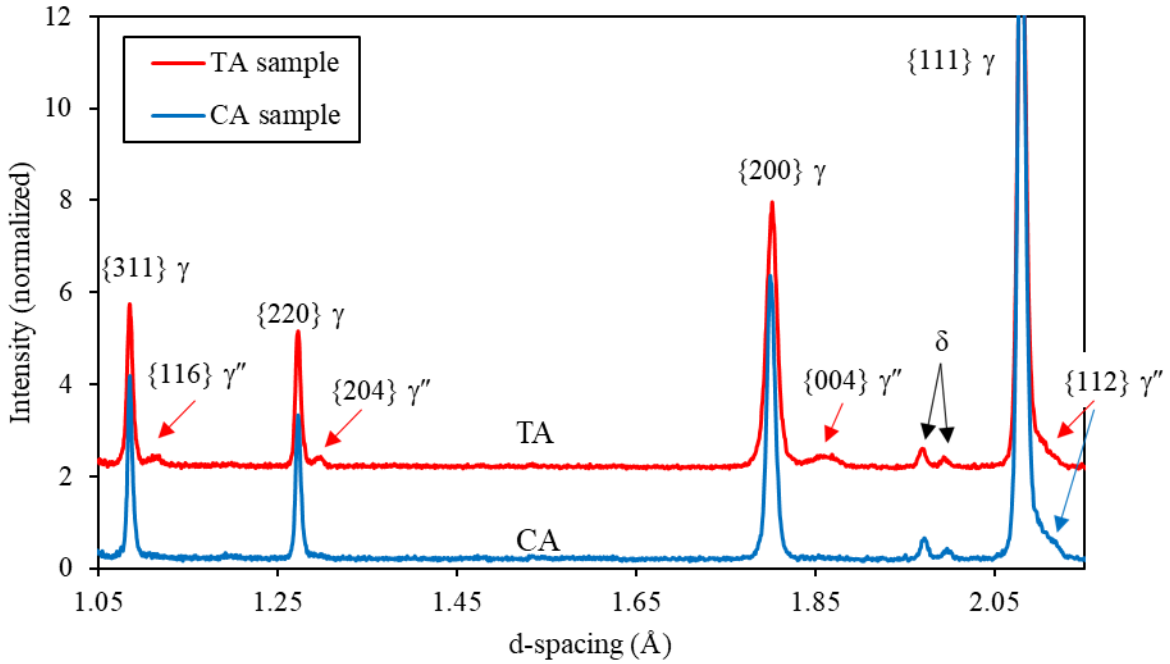

Figure 4. Diffraction patterns obtained along the loading direction at room temperature (RT) before loading of both tensile-aged (TA) and (compressive-aged) CA samples. Small {116}{204}{004} γ" peaks are discerned in TA sample but not in CA sample.

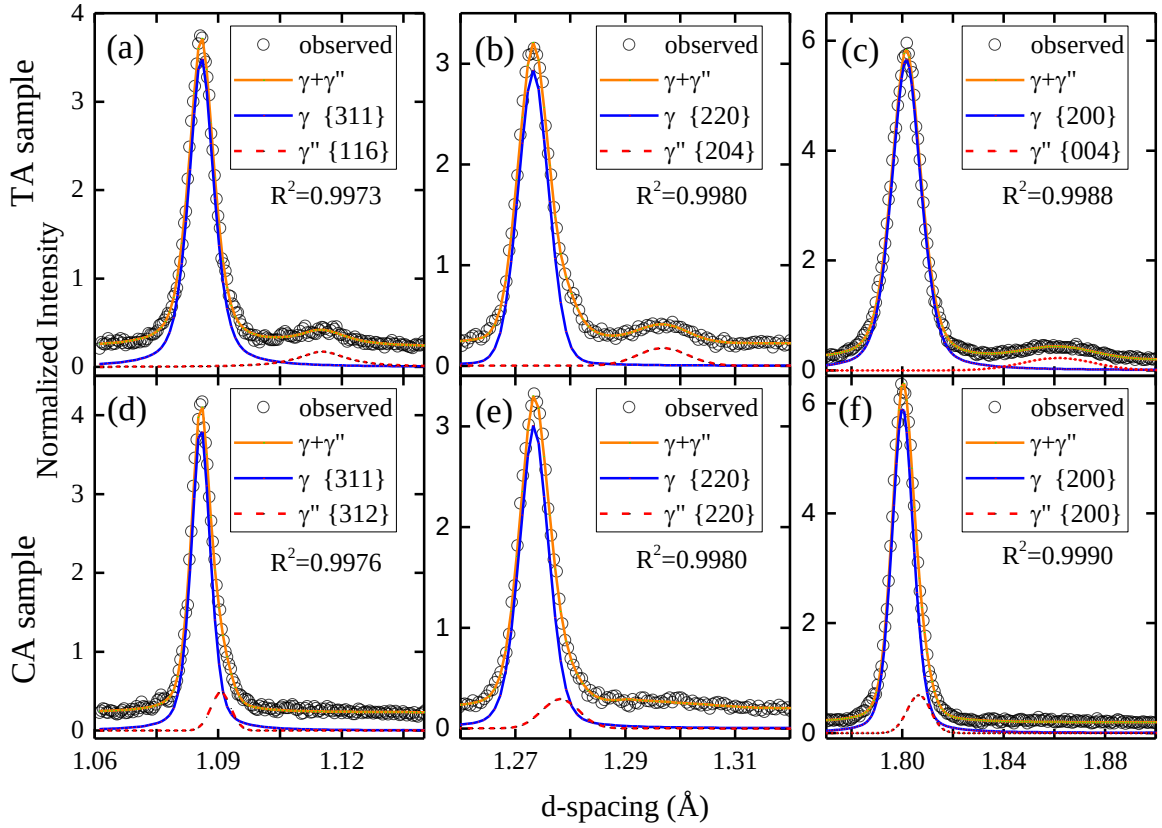

Figure 6. Fitting of diffraction peaks for (a) – (c) non-overlapping peaks for tensile-aged (TA) sample, and deconvolution results for (d) – (f) overlapping peak for compressive-aged (CA) sample, showing the accuracy of the fitting.

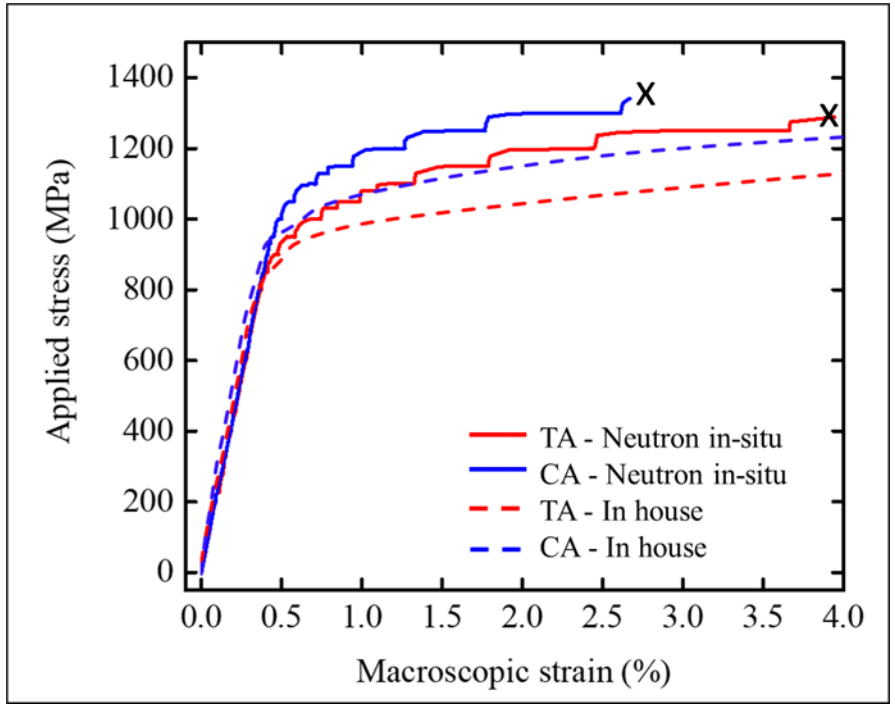

Figure 8. Applied stress-strain curves for quasi-static in situ neutron tensile deformation and in house laboratory tensile deformation of the two differently aged sample. The ‘x’ marker shows the point where the extensometer slipped.

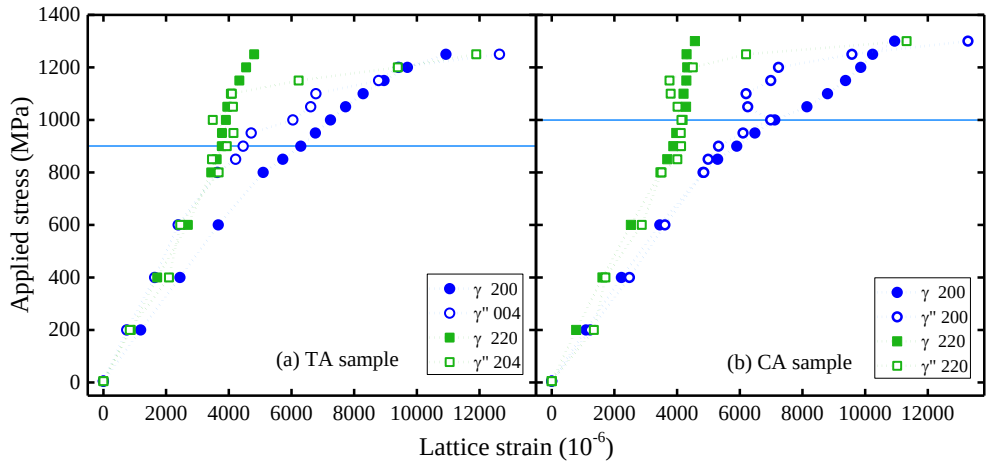

Figure 10. Lattice strain evolution of the γ and γ″ phases for (a) tensile-aged (TA) and (b) compressive-aged (CA) samples during tensile deformation. The horizontal lines indicate the onsets of nonlinearity. Error bars associated with uncertainties of peak fitting are about the size of the symbol in the elastic regime for both phases, and increase from 200 to 1200 microstrains in the plastic regime for the γ″, 100 to 360 microstrains for the γ phase. Error bars are not shown for clarity.

Figure 11

Click here to access/download;Figure;Figure 11.pptx

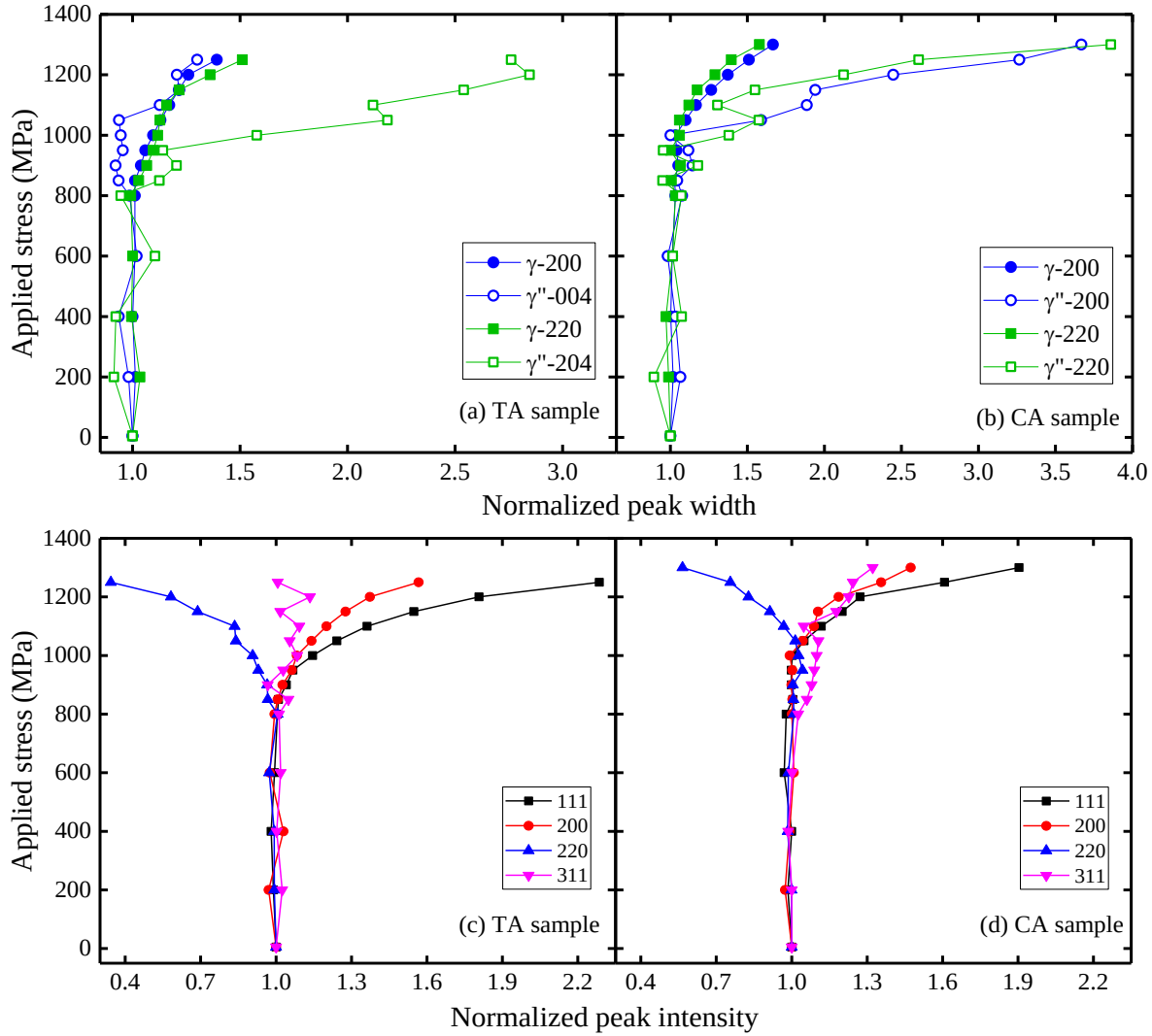

Figure 11. Evolution of normalized peak broadening of the γ and γ″ phases in the {200} and {220} oriented grains for the (a) tensile-aged (TA), (b) compressive-aged (CA) samples. And peak intensity evolution for (c) TA and (d) CA samples. Error bars for peak width associated with uncertainties of peak fitting are about the size of the symbol in the elastic regime, and increase from 0.07 to 0.44 in the plastic regime for both phases. Error bars for peak intensity are about the size of the symbol. Error bars are not shown for clarity.

- This study reveals, for the first time, the micro-mechanism of deformation of γ'' strengthened superalloys using neutron diffraction.
- Inconel 718 samples with different γ'' variant distributions were prepared by different stress ageing heat treatments.
- The γ'' variant-sensitive deformation behavior was studied by interpreting the stress-lattice strain curves.
- Compressive-aged sample shows larger yield strength compared to the tensile-aged sample
- The difference in strengthening arises from the interactions between dislocations and different γ'' variants.

Graphical Abstract

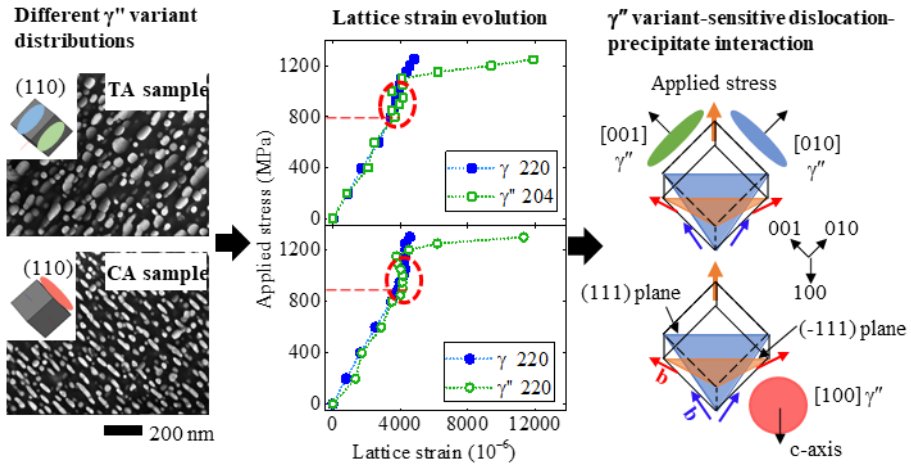

Hongbiao Dong
Professor of Materials Engineering
Research Chair of Royal Academy of Engineering
Department of Engineering
University of Leicester
University Road, Leicester
LE1 7RH, UK

March 14, 2022

Editor
Journal of Materials Science & Technology

Subject: Ref. No.: J-MST-D-22-00454
Title: γ" variant-sensitive deformation behaviour of Inconel 718 superalloy

Dear Editor,

Thank you for your email with the detailed comments of the two Reviewers. We found the comments very fair and constructive. In accordance, we have drafted a detailed response to every comment, as outlined in the letter below and also indicated where within the manuscript these responses have been incorporated. Within the revised manuscript, these responses are highlighted in red font to highlight them from the initial text. They have also been included in this response letter and appear in blue font.

I hope that these responses and amendments satisfactorily and adequately address the queries and clarifications that were sought by the two Reviewers. Moreover, we trust that you now find the manuscript in an appropriate form that is deemed suitable for publication as a technical **article in your journal.**

I hereby certify that all the authors have agreed to the submission of this revised manuscript. I hope you find all in order and I look forward to hearing from you.

Yours sincerely,

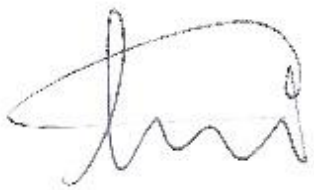

Hongbiao Dong (Corresponding author)

Detailed Response to Reviewer's Comments

Reviewer #1:

The present work deals with the role of applied stresses during ageing on the growth of g'' precipitates in IN718 and the resulting deformation mechanisms on the microscale. Neutron diffraction technique was applied after heat treatment to study the evolution of micro strains in the g matrix as well as in g'' precipitates during macroscopic plastic deformation. This is a very good work and only a minor revision is suggested:

Line 83: „a post-mortem microstructures" - please correct the language

Line 93: ", where" - The "," is not used in Eq. (2) and (3). Please use the "," consistently throughout the text.

The font size is not consistent - especially between Line 97 and 106.

Authors: thank you for pointing out the typo errors, the errors have been corrected in manuscript now.

Section 2.2: What was the step size and spot size used for electron microscopy. The precipitates are of nanometre size and exact examination is limited by not seeing smaller precipitates.

Authors: For the SEM characterisation, the voltage used was 5kV with probe current 5x10^-11 A, the resolution is about 1.5 nm. The g' precipitates were observed to be 20-30 nm, if there were particles in size smaller than this, they should be observed under this resolution.

Figure 2 and the explanation given in section 2.2 have to be shifted to the results part. This is the methodology section.

Authors: thanks for the suggestion, this part is now shifted to result section.

What about the co-precipitation of y' and y'' forming sandwich-like structures. What is their role on the strength or what will they change with respect to the results found in the present work?

Authors: it will be very interesting to investigate the situation of g'-g" compact or sandwich-like morphology. The literature suggests the compact morphology will lead to higher strength and better thermal stability as the presence of g' in higher volume fraction and compact morphology will require more complex dislocation structures to plastically deform the material and hinder the coarsening of g". The deformation mechanism in materials with compact morphology would be different from the conventional IN718, in which strength is considered largely arises from coherency strengthening. The compact morphology can have a very different strain field around the co-precipitates compared to monolithic morphology, in addition the higher g' volume fraction contributes

additional strengthening. It will be interesting to investigate the underlying mechanism during deformation with in-situ neutron diffraction, however, it will be very difficult to deconvolute the overlapping peaks from the three phases. The stress-ageing method used in this study may still validate in tailoring the presence of specific variant of g", this may favour the deconvolution of overlapping peaks in particular situations.

Please take care that the curves in all Figures can also be distinguished when printing in black and white.

Authors: thank you for the suggestion, changes are made to Figure 4, 6, 8, 10 and 11.

In Figure 8b no unit is given on the x axis. For a better comparability, both x axis in a) and b) should be in %. I would also suggest to merge Figure 8a and b.

Authors: that's a good suggestion, the figures are merged for a better comparability.

Reviewer #2: Favor:

1. The topic to explore the effect of gamma double prime with certain orientation in IN718 is interesting. It provides a possible way to engineer an IN718 with increased strength, which would be attractive to additive manufacturing industry where high level of residual stresses exist.
2. The yield strength is higher for the sample aged in compression compared to the ones aged in tension, the difference in yield strength by different stress ageing (compression or tension) show consistency between laboratory tensile test and in situ neutron experiment: It is interesting that the authors point out the effects of stress ageing are opposite when comparing polycrystalline IN718 (this experiment) against single crystalline IN718 (Oblak's experiment). The hypothesis of dislocations shearing certain variant of gamma double prime in certain oriented grains associated with coherency strengthening theory seems well explains the findings.
3. The way to generate gamma double variant distribution with stress ageing is interesting. Its formation and effect seem have been studies systematically in a series of publications by the authors. In this paper, the correlation between microstructure tailoring, macro-mechanical properties and grain level mechanical properties are well presented and convincing.

Authors: thank you for the positive comments.

Distractive:

1. It is a pity that there was no micrograph to show the evidence of dislocations activities to support the hypothesis of the variant sensitive dislocation-precipitate interactions. I understand that such a characterization can be very challenging especially when sample is strained to 3-4%.

Authors: Thank you for pointing out his important point. A more detailed microstructure analysis will be performed in future, with samples slightly plastically deformed to different strain (i.e. 1-2%) before extracting TEM foils. We also consider to use ECCI imaging using the Merlin with its highly parallel electron beam to investigate micro-scale deformation.

2. Table 5 states that the volume fraction of gamma double prime is only 8%, which seems to come from the neutron diffraction experiment, though no information has been given about the exact fitting procedure. The number is a bit lower for IN718 as normally the volume fraction of gamma double prime in an aged IN718 is considered to be ~15%. The authors may need to explain the low volume fraction issue and better to let the reader know about the typical volume fraction in the literature.

Authors: The f is derived from the intensity of {220} γ peak and {204} γ″ peak from neutron diffraction of the TA sample with scattering structure factor taken into account:

$$\frac{I^{\gamma''}}{I^{\gamma''}} = \frac{(\lambda^{\gamma''})^3(\eta_{\gamma''})^2 f_{\gamma''}}{(\lambda^{\gamma})^3(\eta_{\gamma})^2 f_{\gamma}} \qquad (4)$$

, where I is the intensity, λ is the wavelength of diffraction neutron beam, η the scattering density, the detailed calculation is referred to a previous study in ref. [30].

3. The authors should describe in more detail how variant selection of gamma double prime makes the neutron diffraction peak of the phase more discernible, it would be good to describe it in 2-3 sentences. There is also no mentioning of the superlattice reflection that is produced by gamma double prime when studied by electron microscopy and synchrotron x-ray diffraction.

Authors: For a sample without variant selection, two diffraction peaks of gamma double prime exist due to the different lattice parameters along a- and c-axes. In contrast, for a variant selected sample, the gamma double prime diffraction peak includes all the intensity arises from the precipitates' volume in these grains and have higher intensity

The superlattice peaks by election diffraction and synchrotron x-ray are an indication of the existence of precipitates, and even the existence of different variants of gamma double prime. But the neutron diffraction in this study has a unique advantage compared to electron or synchrotron. The neutron experiment was setup to align the diffraction vector parallel to the longitudinal direction of the sample, such a setup allowed the obtained diffraction peaks to came from the grains with close orientation to the grains shown in the SEM images. Which means the diffraction peaks have a good correlation with the observed microstructures, this is important as the peak represent the lattice spacing of grains and specific gamma double variants with a specific orientation to the stress-axis. And this will be difficult to achieve by either electron or synchrotron diffraction if it is not impossible.

Importance of contribution:
The paper has studied the effect of different gamma double prime variant distribution on

strengthening of IN718, and based on the result, suggested a possible way to tailor the gamma double prime variant distribution that will increase the yield strength of IN718.

Based on the quality of the paper and its potential contribution to the literature, I recommend publication of the article in Journal of Materials Science and Technology after minor revising.

Authors: thank you for your kind acknowledgement.